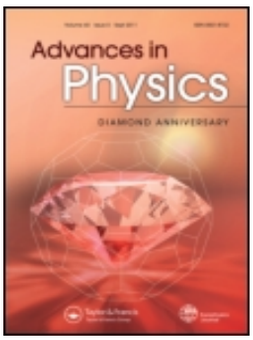

Advances in Physics

ISSN: 0001-8732 (Print) 1460-6976 (Online) Journal homepage: http://www.tandfonline.com/loi/tadp20

Mean-field theory of intermediate valence/heavy fermion systems

D.M. Newns & N. Read

To cite this article: D.M. Newns & N. Read (1987) Mean-field theory of intermediate valence/heavy fermion systems, Advances in Physics, 36:6, 799-849, DOI: 10.1080/00018738700101082

To link to this article: http://dx.doi.org/10.1080/00018738700101082

Published online: 02 Jun 2006.

ADVANCES IN PHYSICS, 1987, VOL. 36, NO. 6, 799–849

Mean-field theory of intermediate valence/heavy fermion systems

By D. M. NEWNS
IBM T.J. Watson Research Center, P.O. Box 218,
Yorktown Heights, NY 10598 U.S.A.

and N. READ
Department of Physics, Massachusetts Institute of Technology,
Cambridge, MA 02139 U.S.A.

[Received 1 June 1987]

Abstract

In recent years the class of materials known as intermediate valent, Kondo-lattice or heavy-fermion systems has aroused much interest. The unusual properties of these materials arise from the behaviour of their 4f- (or 5f-)electrons. The strong electron–electron interactions within the 4f shell cause the f-bands of these rare earth or actinide metal containing species to show very high masses. Thus the densities of states are very high, leading to correspondingly high specific heats and magnetic susceptibilities. A mean field theory is described, based on the Anderson lattice model, in which these properties are straightforwardly explained. Its relationship to the $1/N$ expansion, and the corrections to mean field, are outlined.

Contents

1. Introduction

1.1. *Generalities*

In recent years a class of rare earth (RE) and actinide materials has become widely studied, termed variously intermediate valent, Kondo-lattice or heavy-fermion systems [1–5] (e.g. $CeSn_3$, YbCuAl, SmS, $CeAl_3$, UBe_{13}). In these materials the 4f- or 5f-electrons are itinerant as are the d-electrons in transition metals. However, the very strong electron–electron interaction within the tightly bound 4f shell [6, 7] seems to be the reason why the f-bands in these materials show high to extremely high masses. Accordingly, densities of states in metallic, non-magnetic systems are very high, leading to very high specific heats and susceptibilities. The linear coefficient of specific heat at $T = 0$, γ, may vary from 0·01 to $1\,J\,mol^{-1}\,K^{-2}$ in this range of materials, compared with 1 to $10\,mJ\,mol^{-1}\,K^{-2}$ for ordinary metals [9]. When $\gamma \gtrsim 0{\cdot}5\,J\,mol^{-1}\,K^{-2}$ the heavy-fermion label tends to be applied, or maybe the appellation Kondo lattice in the case of a Ce material. Intermediate valent (IV) materials are essentially rare earth materials with a somewhat lower γ than the heavy fermion materials, but still much greater than a conventional metal. Examples of insulating systems (SmS, SmB_6) also exist [2]. In this case, the high effective mass manifests itself as an exceedingly narrow energy gap.

Despite the common property of having electrons in relatively narrow bands, the properties of the materials with strongly correlated f-electrons have little in common with transition metals. In the transition-metal materials a magnetic phase transition seems to be the consequence when electron–electron interactions become stronger than a critical value. Mass enhancements are moderate. On the other hand, the f-electron itinerants show large to huge mass enhancements. When magnetism occurs, it is of a rather different (Ruderman–Kittel mediated, RKKY) type to the Stonor–Wohlfarth magnetism of transition metals, and seems to indicate a partial breakdown in f-electron itinerancy.

Indeed the f-electron itinerants tend to have a lot in common with magnetic (4f- or 3d-) impurities. The impurities have a low characteristic temperature or energy scale T_K [9]. Because T_K is given by a formula of the type $T_K \sim A \exp(-1/b)$, where b is positive but less than unity, T_K can be exceedingly small. Hence the Pauli susceptibility and Sommerfeld specific-heat coefficient γ, which go as T_K^{-1}, can be extremely large. Giant thermopowers are seen, [10] etc. In fact for the IV materials one can pursue the analogy with impurities to a remarkable level of detail in comparison with experimental data [11].

However, there are many important phenomena which manifest lattice, rather than magnetic impurity behaviour. Resistivity goes like T^2 at low temperatures as

expected in an interacting Fermi liquid [12]. Especially remarkable is the superconductivity of the heavy Fermion materials which seems not always to be of $l = 0$ type at least in some materials [4]. It is believed that the superconductivity is another intrinsic property of the strong interaction between the fermions, as in liquid He^3 [13]. It seems that a new type of theory is needed to explain the properties of the f-electron itinerants, whose electrons suffer such enormous mass enhancement that ordinary concepts of perturbation theory are of little value.

Here we shall describe mainly the IV systems which seem to be better understood at the present time, and especially their low-temperature properties. We shall do this from a particular theoretical point of view, probably the simplest theoretical viewpoint available. Where other approaches overlap or take over, we shall refer the reader to the literature rather than detail them here.

1.2. *Picture of the intermediate valent 4f ion in a metal*

The picture we have of an IV 4f ion in a metal (Hirst 1974) underlies the theoretical models used in the following. We do not know to what extent it might be applicable to a 5f ion such as U. Consider an ion such as Ce. A schematic energy level diagram is shown in figure 1. The Ce ion is normally considered to be stable in two valence states, trivalent, f^1 and tetravalent, f^0. The f^2 state is much higher up in energy because of the Coulomb interaction energy [14, 15]

$$U_{mn} = \int \psi^*_{4fm}(1)\psi_{4fm}(1)\frac{1}{|\mathbf{r}_1 - \mathbf{r}_2|}\psi^*_{4fn}(2)\psi_{4fn}(2)\,d\mathbf{r}_1^3\,d\mathbf{r}_2^3 \approx U \qquad (1)$$

between two electrons occupying a wavefunction ψ_{4fm}, of magnetic quantum number m, on the same atom. The expression (1) overestimates U for two reasons. First the electrons move around in the densely occupied 4f shell so as to increase their

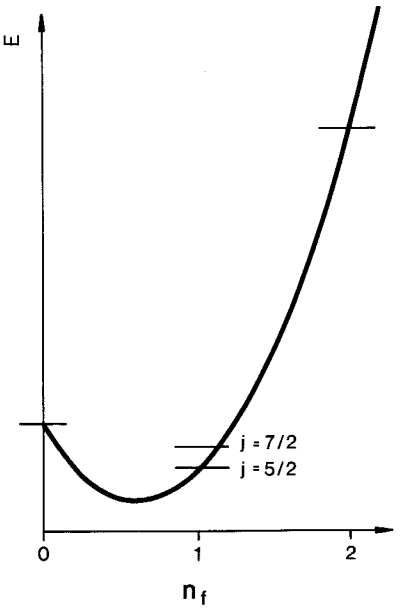

Figure 1. Schematic plot of ground-state energy E of a Ce atom in a metal as a function of number of electrons n_f in the 4f shell.

separation, an intra-orbital correlation effect. Secondly, the extra electron in the 4f brings with it a screening cloud in the metal, which lowers the energy of $4f^2$. Nevertheless, if the energy of the $4f^1$ state is E_f, that of the $4f^2$ state may be written $2E_f + U$, where U measured experimentally in a metallic environment [6, 7] is about 5–8 eV. This estimate may be taken to include the intra- and extra-orbital screening effects.

It is then usually considered that if the f^0 and f^1 states are reasonably close together (say up to ~ 2 eV difference), the high-lying f^2 state, and the even higher-lying f^3 states, are too high up to be included. The theory then assumes that this system is confined in the f^0–f^1 subspace. The f^0 state is non-degenerate. However, the f^1 state is 14-fold degenerate, split by the spin-orbit interaction into a 6-fold degenerate $j = 5/2$ ground state and an 8-fold degenerate $j = 7/2$ excited state about 300 meV higher up. Usually theory not only neglects the f^2 state, but also the $f^{7/2}$ excited state, so that the subspace is reduced to include only f^0 and the $j = 5/2$ subspace of f^1.

In table 1 we list details of the commonly intermediate-valent ions; Ce, Sm, Eu, Yb and Tm. All but Tm have one state non-magnetic, and one magnetic, like Ce. Also, Ce f^1 and Yb f^{13} have their ground states ($j = 5/2$ and $7/2$ respectively) well separated from the excited states, but there is a much smaller separation for Eu and Sm. We also list the g-factors of the ion which are important in calculating the magnetic susceptibility.

In addition to the spin–orbit splitting, a crystal-field splitting of the ground-state multiplet may occur [3–5]. This is likely to be especially important for systems with a very low energy scale, i.e. very high γ, such as occurs in heavy fermion/Kondo-lattice systems. Some of these systems approach a situation where the limit for a ground-state doublet or quadruplet is more appropriate than the full multiplet (e.g. $N = 6$ for Ce).

Next we consider how the valences f^0 and f^1 for cerium are coupled together. We imagine that one RE ion is located in a free-electron gas (jellium), whose eigenstates are usually taken in spherical coordinates (assume these are stationary states in a large spherical box) as $|k, l, l_z, \sigma\rangle$, where k is the radial quantum number, l = total orbital angular momentum, l_z is its z-component and σ = spin. However, we prefer to reorganize these states into $|k, j, m,\rangle$, where $j = l \pm 1/2$ and $-j \leqslant m \leqslant j$,

$$|k, j, m\rangle = a|k, l, l_z - \tfrac{1}{2}, \uparrow\rangle + b|k, l, l_z + \tfrac{1}{2}, \downarrow\rangle, \tag{2}$$

where a and b are Clebsch–Gordon coefficients. The location of the RE atom at the center of the jellium sphere allows mixing between states of the same quantum number

Table 1. Details of the commonly intermediate valence ions; J is the ground-state spin and g is the gyromagnetic ratio, which is important for calculating the magnetic susceptibility.

Configuration	RE ion	J	Fermions	g	$g^2J(J+1)$
f^0–f^1	Ce	5/2	e	6/7	6·43
f^6–f^5	Sm	5/2	h	2/7	0·71
f^6–f^7	Eu	7/2	e	2	63·0
f^{14}–f^{13}	Yb	7/2	h	8/7	20·57
f^{12}	Tm	6		7/6	57·2
f^{13}	Tm	7/2	h	8/7	20·57

on the atom and in the jellium, giving matrix elements

$$V_k = \langle f^1, 5/2, m|V|f^0, k, 5/2, m\rangle, \tag{3}$$

where V is the coupling perturbation.

We now attempt a fermionic representation of the model so far. The resulting 'Infinite-U Anderson model' is (taking Fermi level as energy zero)

$$H = E_0 \sum_m f_m^\dagger f_m + V \sum_{k,m} (f_m^\dagger c_{km} P_0 + c_{km}^\dagger f_m P_1). \tag{4a}$$

Here f_m is a Fermion operator describing the state of angular momentum m of f^1, and c_{km} is the operator describing $|k, 5/2, m\rangle$. E_0 is the energy difference $E(f^1) - E(f^0)$. V is the matrix element (3) with k-dependence dropped. P_0 is a projection operator onto the f^0 state and P_1 is a projection operation onto the f^1 state. Without these projection operators, forbidden states f^2, f^3 would be generated by the successive action of $f_m^\dagger$ on f^0.

Equation (4a) applies to Ce compounds. It may be applied to Yb compounds by taking $j = 7/2$, and making an electron–hole inversion (since the valences of Yb are f^{13}, f^{14} its magnetic configuration has one hole). For Sm materials one may use (4) with electron-hole inversion and $j = 5/2$, and Eu with $j = 7/2$ and no inversion, but in the last two cases caution is needed because of the narrow gap from the ground state to the first excited-state multiplet.

Finally, we should mention that there exists a 'Kondo limit' of (4a) when E_0 becomes large and negative, and the f^1 state behaves like a spin. Charge fluctuations to f^0 are suppressed and the model describes a spin j interacting with an electron gas via an exchange interaction $J = V^2/E_0$. The resulting SU(N) f^1 Kondo, or Coqblin–Schrieffer [16] model may be derived from (4a) by a Schrieffer–Wolff transformation, to give

$$H = \sum_{k,m} \varepsilon_k c_{km}^\dagger c_{km} - J \sum_{kk'mm'} c_{k'm'}^\dagger f_m^\dagger f_{m'} c_{km}. \tag{4b}$$

1.3. *Phenomenology*

In this article we consider systems which have normal Fermi-liquid ground states. Let us concentrate on systems in which crystal fields do not split the ground-state multiplet significantly, i.e. the IV rather than the heavy fermion or Kondo-lattice systems.

First let us draw attention to some remarkable scaling properties approximately obeyed by IV systems [17–19]. To provide some motivation, imagine for a moment that they consist of non-interacting electrons and that the rare earth ions are non-interacting impurities. The linear coefficient of specific heat per RE site at $T = 0$, γ, is given in a non-interacting electron gas by

$$\gamma = \frac{\pi^2}{3} k_B^2 N \varrho_f, \tag{5}$$

where ϱ_f is defined as the density of states per RE atom per channel m for our impurity in the electron gas, and $N = 2j + 1$ is the number of channels.

Now we apply a magnetic field h, yielding a Zeeman term in the Hamiltonian (using spherical symmetry around each ion)

$$H_Z = g\mu_b \sum_m m n_{fm}, \tag{6}$$

where $n_{fm} = f_m^\dagger f_m$, g is the g factor and μ_B the Bohr Magneton. We neglect coupling to the non-f electrons whose susceptibility is small. The linearly induced f-polarization in the mth channel will be $\delta\langle n_{fm}\rangle = hg\mu_B \varrho_f m$. Hence the moment is

$$M = g\mu_B \sum_m \delta\langle n_{fm}\rangle = hg^2\mu_B^2 \varrho_f \sum_m m^2. \tag{7}$$

Therefore, the susceptibility $\chi = \partial M/\partial h$ is

$$\chi = N(\mu_{eff}^2/3)\varrho_f, \tag{8}$$

where we define

$$\mu_{eff}^2 = 3g^2\mu_B^2 \sum_{m=-j}^{j} m^2 = g^2\mu_B^2 j(j+1). \tag{9}$$

From (5) and (9), we see that there should be a proportionality

$$\frac{\chi}{\mu_{eff}^2} = \frac{\gamma}{\pi^2 k_B^2} \tag{10}$$

for all materials in this class. In figure 2 we plot [17, 18] the two sides of (10) for a number of materials (we have not attempted to bring the plot fully up to date) and we see that it is indeed valid despite a wide range of γ and μ_{eff}. This implies something about the electrons in IV systems behaving like non-interacting quasi-particles *and* the rare earth ions behaving a lot like non-interacting impurities. Of course, it does not imply that we really have non-interacting electrons, otherwise γ could never reach the high values observed in many IV materials.

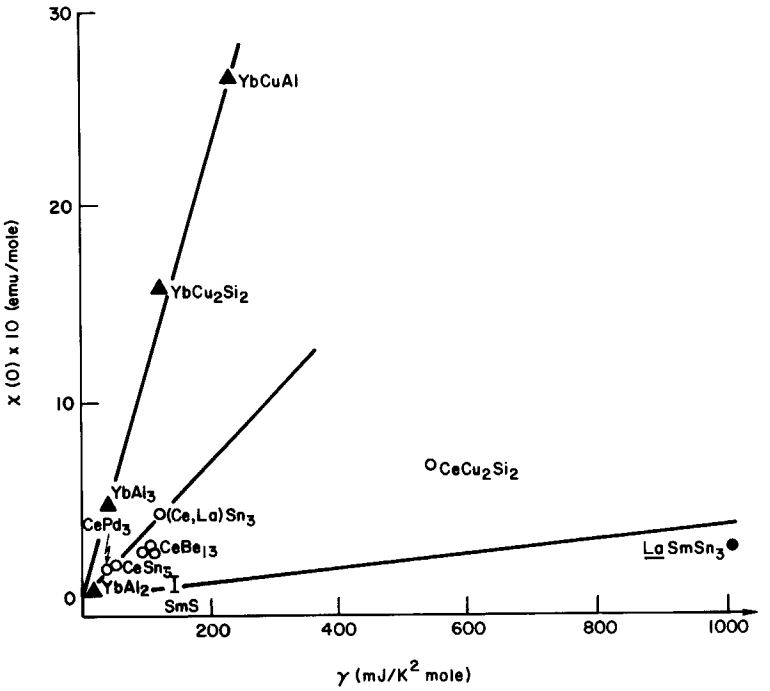

Figure 2. $T = 0$ magnetic susceptibility χ plotted against linear coefficient of specific heat γ for various intermediate valence compounds. Straight lines are equation (37).

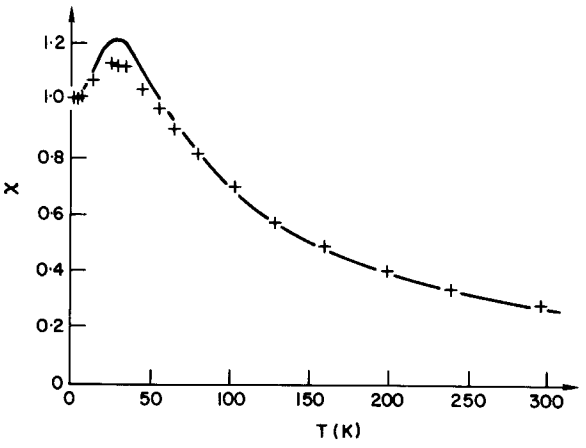

(*a*)

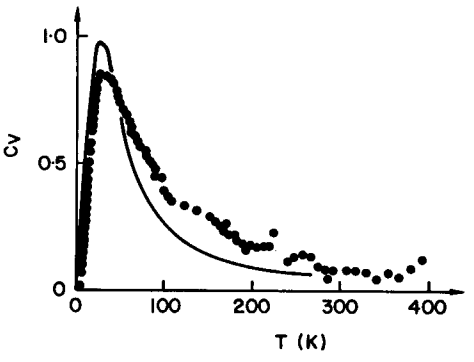

(*b*)

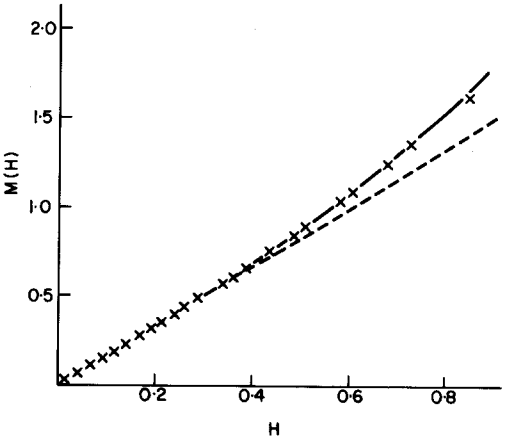

(*c*)

Figure 3. (*a*), (*b*), (*c*) contain, respectively, plots of magnetic susceptibility [20], electronic specific heat [21] and magnetization [20] of YbCuAl against temperature (in (*a*), (*b*)) or magnetic field (*c*). The continuous curve is the exact solution of the 8-channel Kondo model ($n_f = 1$) [22, 23] with $T_\chi = 100\,\mathrm{K}$ (equation (12)), $T_K = 98\,\mathrm{K}$ (equation (44)).

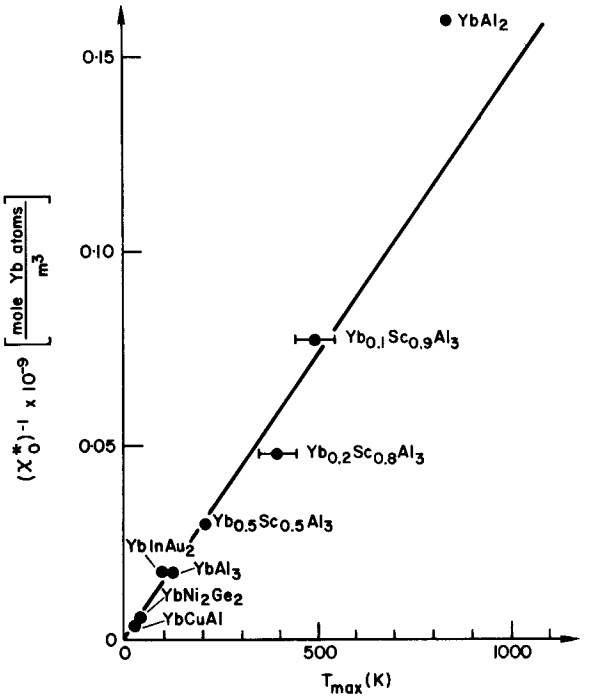

Figure 4. Plot of the inverse of $T = 0$ magnetic susceptibility, χ^{-1}, against temperature $T_{\max}$ of the maximum in $\chi(T)$, after [19].

Next consider the plot of χ against temperature [20] in figure 3 (*a*), where results are illustrated for YbCuAl. We see that χ at low temperatures is constant, the Pauli susceptibility just considered. At high temperatures, χ has the Curie-type behaviour

$$\chi = (\mu_{\text{eff}}^2/3k_B T). \tag{11}$$

At intermediate temperatures χ has a maximum, which is characteristic of IV materials. The general behaviour of $\chi(T)$ illustrated in figure 3 (*a*) is typical, only $\chi(0)$ and the temperature $T_{\max}$ at which χ peaks being characteristic of individual materials.

Let us now plot $\chi_0 \equiv \chi(0)$ against $1/T_{\max}$, as done in figure 4 [19]. We see that there is a clear *scaling*: systems with large χ_0 have small $T_{\max}$ (e.g. YbCuAl), and the reverse is also true.

Another correlation is between $\chi(0)$ and the average number of f-electrons $\langle n_f \rangle = \Sigma_m \langle f_m^\dagger f_m \rangle$, i.e. the mean valence. This plot is shown in figure 5 for ytterbium materials [19]. There are inaccuracies in the $\langle n_f \rangle$ measurements, but it is seen that systems with large χ_0 are close to the magnetic (f^{13} for Yb) valence, and systems with small χ near to the non-magnetic (f^{14}) valence.

We see that there is a remarkable *universality* in the properties of IV systems [17–19]. They can be approximately categorized by a single number, a susceptibility χ_0, or equivalently an energy scale $T_{\max}$, which varies systematically with valence. If $T_{\max}$ is known, one can predict χ_0 and γ.

Finally we shall see that the individual curves of $\chi(T)$ [20], electronic specific heat $C_v(T)$ [21] and magnetization $M(h)$ [20] illustrated in figure 3 for YbCuAl can even be understood in detail on the basis of the impurity model. We start from

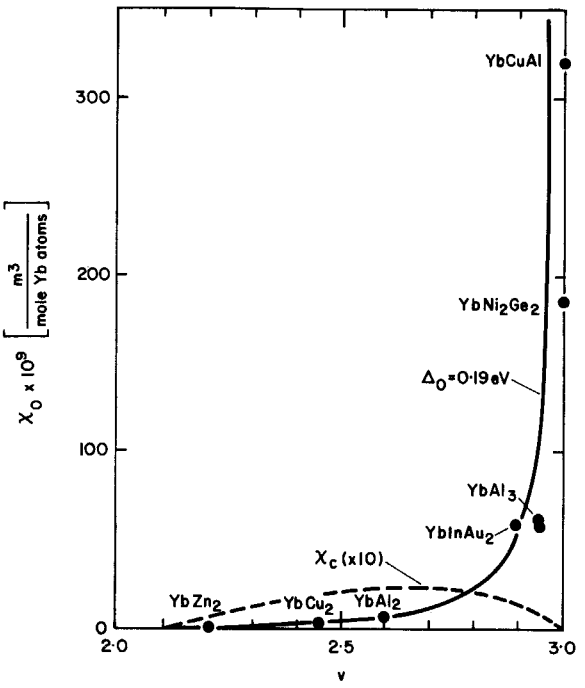

Figure 5. Plot of $T = 0$ magnetic susceptibility against valence for Yb intermediate valence (IV) compounds, after [19]. Full curve is equation (35) with $\Delta_0 = 0{\cdot}19$ eV; broken curve is χ_c from (38).

the model (4), the Infinite-U SU(N) Anderson model. This model has been exactly solved by Bethe *ansatz* techniques [22–28]. The remarkable solution is difficult and technical [22–27], and we shall not dwell on it here. However, we shall quote the results.

First of all we note that YbCuAl is found experimentally to lie exceedingly close to the f^{13} limit (figure 5). Therefore (given that apart from having $j = 7/2$ this one-hole system is equivalent to f^1 cerium), Yb in YbCuAl is capable of being treated in the Kondo limit [22–26], i.e. by (5*b*) rather than by (5*a*). In the Kondo regime the model has only one characteristic energy scale T_K, the Kondo temperature, which may be defined as T_χ in

$$\chi(0) = \tfrac{1}{3}g^2\mu_B^2 j(j+1)/T_\chi. \tag{12}$$

(Another temperature $T_0 = NT_\chi$ is also frequently introduced. Wilson's characteristic energy scale T_W in the high-temperature region is $T_W = T_\chi \exp(1 + C - 3/2N)/2\pi\Gamma(1 + 1/N)$ where C is Euler's constant and Γ the Gamma function.) When this is done [29] all the other thermodynamic properties, $\chi(T)$, specific heat $C_v(T)$ and magnetization $M(h)$ at $T = 0$ are seen to fit remarkably well [29] (see figure 3). YbCuAl is seen to have impurity-like thermodynamics.

We now turn to developing approximate solutions to our model (4). We are motivated partly by a desire for pedagogical simplicity. Additionally, there are non-thermodynamic properties (photoemission spectra, transport properties) which cannot be calculated within the Bethe *ansatz* technique even for one impurity. Most important however, we wish to develop the theory of the lattice, which unlike the single RE impurity is not exactly soluble. Such a solution should clearly help us to

understand the impurity-like thermodynamics and scaling properties which have been alluded to in this section. Furthermore it should give a coherent ground state and enable transport properties like the T^2 resistivity at low temperatures and the thermopower to be calculated.

In addition, a goal is to understand the Tm ion as an impurity and in a lattice situation such as TmSe. This ion poses problems because of the degeneracy of both valences. It is hoped that study of this ion will be helpful in understanding the very important uranium materials, since the U ion, usually considered to be f^2–f^3, poses similar problems.

1.4. *Origins of mean field, 1/N expansions*

In many areas of condensed matter physics a step forward has been taken when the mean-field solution to a particular problem was identified. In the case of (4) and its relatives the mean-field solution has been found in the last few years and it does seem to provide a foundation upon which basic understanding of the intermediate-valent and heavy-fermion state may rest.

The origins of this development lie in early work by Yoshimori and Sakurai [30] in 1970 on the spin-$\frac{1}{2}$ Kondo problem. This predates Wilson's solution [9], and had these authors correctly calculated the χ/γ ratio by introducing Gaussian fluctuations, as they nearly did, the understanding of the Kondo problem would have been advanced by several years. However, their solution may have seemed an arbitrary approximation at that time.

Lacroix and Cyrot [31] extended these ideas to the lattice of spin-$\frac{1}{2}$ Kondo impurities and first developed many ideas which form the centre of this article. Up to this point, the mean-field solution to the spin-$\frac{1}{2}$ Kondo impurity and lattice remained curiosities. However developments were in train which were to change this, involving the use of $1/N$ expansion techniques in attacking models such as (4). The nomenclature here involves a degeneracy factor N, which in our problem is $N = 2j + 1$, and is the degeneracy of the magnetic configuration of the 4f ion. The general principle of a $1/N$ expansion is first to find the diagrams which have the maximal number of internal summations over m (i.e. degeneracy factors N) in each order. These form the leading-N approximation. Higher-order approximations may also be feasible by summing diagrams with next-to-maximal number of internal summations, etc.

An approach to the solution of (4*a*) existed by using a non-Feynman diagram technique invented by Keiter and Kimball and independently by Hewson and Movaghar. The technique was first applied to the present problem by Bringer and Lustfeld [17]. Ramakrishnan and Sur [34] showed how this could be organized into finite summable classes of diagrams by use of the $1/N$ expansion concept, and many others followed in his footsteps [35, 36]. Identical expressions were obtained by a variational procedure [37]. When the dust had settled it was realized, by careful comparison with the exact solution to (4) [36] that the Ramakrishnan–Keiter–Kimball approach correctly gave the first two orders in $1/N$ in the expansion of calculated quantities. Since $N = 6$ or 8 in IV systems, this is an adequate accuracy for many purposes.

A little after Ramakrishnan and Sur, Read and Newns [38], picking up an idea of S. Chakravarty (unpublished preprint) set out to solve (4) in the Kondo limit (4*b*) by a $1/N$ expansion technique. In their technique, the leading order in $1/N$ is the mean-field theory, and the next order is represented by the fluctuations around mean field. For the first time in a $1/N$ technique, they were able to derive the χ/γ ratio

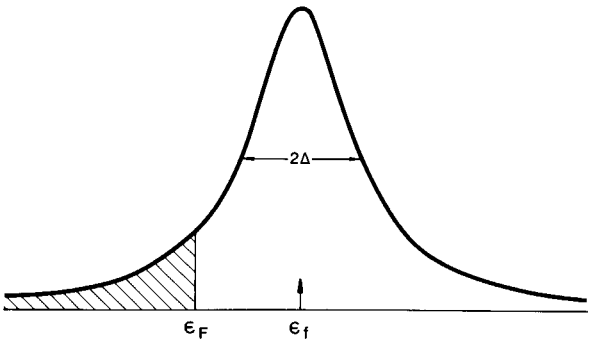

Figure 6. Plot of quasi-particle density of states (22) for a Ce impurity with $n_f \simeq 1$.

correctly, the goal so nearly reached in 1970 by Yoshimori and Sakurai [30]. The mean-field approximation had emerged into clear definition as the leading term in a $1/N$ expansion, and deviations between mean field and exact results could be identified as $1/N$ corrections.

Finally the necessary extension to make treatment of the full Hamiltonian (4*a*) possible opened up with Piers Coleman's 'slave boson' trick [39]. Now mean-field approximation [40] and the $1/N$ corrections [40, 41] for the full Hamiltonian (4*a*) were worked out. Whereas the Keiter–Kimball technique has proved extremely difficult to apply to the lattice, a way to treat the lattice of IV ions had now been opened up. Mean field [43, 42] and recently $1/N$ correction calculations have been done extensively on the lattice [41–45].

In mean field the solution to (4) [38, 40] is just a narrow quasi-particle resonance at the Fermi level. Its shape is Lorentzian, its degeneracy $N = 2j + 1$, and it satisfies the Friedel sum rule in that its occupied area holds $\langle n_f \rangle$ electrons (figure 6). The centre of the resonance is located at T_K above ε_F. The density of states per channel at ε_F in the resonance is to be identified with ϱ_f in the phenomenological approach of equations (5)–(10).

In the case of lattice models, the mean-field theory gives a renormalized or quasi-particle band structure [42–45]. The ground state is coherent. In the case of insulating IV systems (SmS . . .) [43, 46], this allows for a picture in terms of a conventional insulator in which bands below the gap are filled, and bands above it are unoccupied, except that the gap can be very narrow, as indeed is observed.

Finally, we come to the anomalous case of Tm [47, 48], with both valences magnetic, and for this a different type of mean-field solution has to be developed, as described for the first time in this paper.

In the following we shall consider these topics in more detail, starting with the Anderson impurity model (4*a*), then considering two impurities, various lattice models, and finally thulium.

2. Anderson impurity

2.1. *Bosonized model*

The basic model for the large-N treatment is the infinite-U Anderson model (4). This is most conveniently written in terms of the Coleman bosons [39] as

$$H = E_0 \sum_m f_m^\dagger f_m + H_0 + V \sum_{k,m} (f_m^\dagger c_{km} b + c_{km}^\dagger f_m b^\dagger), \qquad (13\,a)$$

where

$$H_0 = \sum_{k,m} \varepsilon_k c^\dagger_{km} c_{km}.$$

In (13 *a*), the bosons have replaced the projectors in (4 *a*); they work as follows. Suppose the system is in a state $|b^1 f^0\rangle$, by which we mean one boson, zero f-electrons. Now if (13 *a*) acts on this state, the $f^\dagger_m c_{km} b$ term will convert the state to $|b^0 f^1\rangle$ (the other terms in H leave the state unchanged or annihilate it). Further application of H leads to the $f^\dagger_m c_{km} b$ term annihilating the state $|b^0 f^1\rangle$, but the $c^\dagger_{km} f_m b^\dagger$ returns the $|b^1 f^0\rangle$ state.

Therefore, starting with either $|b^0 f^1\rangle$ or $|b^1 f^0\rangle$, (13) never leaves the subspace of these states. No $f^2, f^3 \ldots$ states are ever created, so the bosons work like the projectors in (4 *a*). But if we had started with a state such as $|b^1 f^1\rangle$, then the forbidden $|b^0 f^2\rangle$ would be created. It is necessary to eliminate such states, and this is done by introducing a *constraint* [40]

$$Q = n_f + b^\dagger b = 1, \tag{13 b}$$

where $n_f = \Sigma_m f^\dagger_m f_m$. In reality, (13 *a*) plus (13 *b*) are equivalent to (4 *a*). In working with (4 *b*), Read and Newns introduced a similar constraint $n_f = 1$. Note that the operator Q commutes with (4 *a*), as n_f does with (4 *b*).

In fact the correct way to handle (13) involves some relatively cumbersome formalism, e.g. path-integral technique, [38, 40] in order to handle the constraint (13 *b*). However, the purpose of the present article is to dwell minimally on such details. We shall try to find intuitive and formally simple procedures to derive the essential results.

2.2. *Large-N approximation*

At low temperatures, it is found adequate to introduce the constraint in an average way [38, 40]. As if introducing a Legendre transformation to a grand canonical representation from a particle-number representation, we go to a new Hamiltonian

$$H = E_0 n_f + H_0 + V \sum_{km} (f^\dagger_m c_{km} b + \text{h.c.}) + \gamma(n_f + b^\dagger b - 1),$$

or

$$H = \varepsilon_f n_f + H_0 + V \sum_{km} (f^\dagger_m c_{km} b + \text{h.c.}) + (\varepsilon_f - E_0)(b^\dagger b - 1), \tag{14}$$

where we redefine $\varepsilon_f = E_0 + \gamma$ as a quasiparticle f-level. If we look for a state of (14) which is stationary with respect to variations in γ, then the constraint $\langle Q \rangle = 0$ will be satisfied for that state.

Now to give an idea of how the selection of diagrams in powers of $1/N$ proceeds, we imagine a Feynman graph expansion for the free energy of (14) in powers of V [38, 40]. This is perfectly possible since only normal boson and fermion operators are found in (14). Some of the diagrams we obtain are illustrated in figures 7 (*a*) and 7 (*b*).

In order to organize the diagrams in powers of N, conventions (which prove self-consistent) are helpful: firstly we take the vertex V as of order $1/\sqrt{N}$. N is the degeneracy $N = 2j + 1$ of the f^1 state, there being N values of m. Secondly, the propagator G^0_f (and of course G^0_k) are considered N-independent. Then we see that figure 7 (*a*) is of order N and is the leading-N diagram. Figures 7 (*b*), (i), (ii *a*), (iii) etc. are of order 1, these are called the Gaussian fluctuation or RPA corrections to mean field [38, 40]. The diagram of (ii *b*) is of even higher order in $1/N$. The two levels,

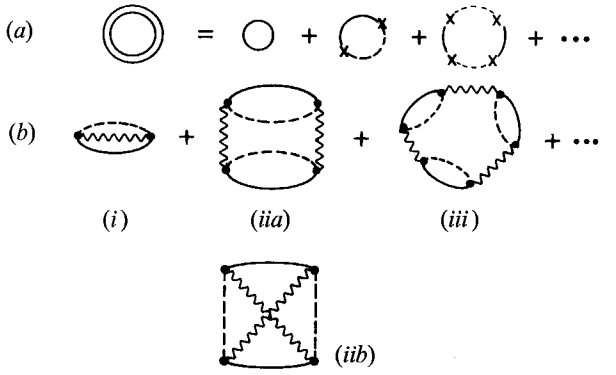

Figure 7. Diagrams contributing to free energy of single impurity. The series (*a*) represent the leading-N diagrams. The diagrams (*i*), (*ii a*) and (*iii*) in (*b*) represent the next order in $1/N$. Diagram (*ii b*) is of still higher order in $1/N$. In (*a*) full line represents bare f-propagator, broken line represents bare k-propagator, cross represents $z^{1/2}V$ vertex. Notation of (*b*) is the same except fermion lines include all $z^{1/2}V$ scatterings, while wavy line represents boson propagator.

figures 7 (*a*) and (*b*), are what have been calculated so far. In fact the assumption that G_f is of order 1 is not strictly valid for the model of (13). But Read [40] has shown that this does not in fact matter: after careful consideration it is found that one can organize the diagrams of figure 7 as if G_f were O(1). Therefore in this article we shall adhere to the large-N procedure which was first used by Ramakrishnan [34].

Another approach is to replace (13 *b*) by the constraint due to Coleman [41] $Q = Nq$, where if we were treating a cerium system $q = 1/6$. Now (13 *b*) only corresponds to an f^0–f^1 model for $N = 6$, but it is argued that the large-N limit may be taken in this new way and then N put equal to 6 at the end, with no less validity than in the conventional procedure. Since the number of f-electrons is now proportional to N (and > 1 for $N \gg 6$), the fractional occupation of the f-level is N-invariant and so G_f may be taken as O(1). We shall not use this procedure here, to keep our large-N procedure the same as that of most of the literature at present.

2.3. *Mean-field approximation: energy scale*

Now in order to get any non-trivial result from figure 7 (a) we need to put in the effect of the bosons in some average way. This is where the *mean-field* concept enters [38, 40]. We replace b and $b^\dagger$ by their expectation values

$$\langle b^\dagger \rangle = \langle b \rangle = z^{1/2}. \tag{15}$$

Now (14) is replaced by the single-particle Hamiltonian

$$H = \varepsilon_f n_f + H_0 + z^{1/2} V \sum_{k,m} (f_m^\dagger c_{km} + \text{h.c.}) + (\varepsilon_f - E_0)(z - 1). \tag{16}$$

The mean-field parameters ε_f and z in (16) are determined by minimizing the free energy of (16). Taking the expectation value, differentiating, and using the Hellman–Feynman theorem $\partial\langle H(\lambda)\rangle/\partial\lambda = \langle \partial H/\partial\lambda \rangle$, where λ is a parameter in H, we obtain

$$z = 1 - \langle n_f \rangle \tag{17 a}$$

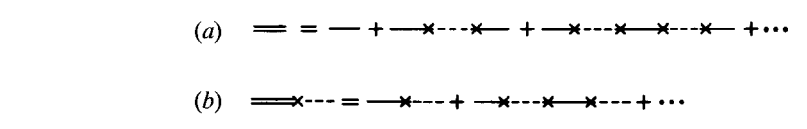

Figure 8. Diagrams contributing to G_f in (21) and G_{fc} in (25); notation as for figure 7(*a*).

and

$$z^{-1/2} VN \sum_k \langle f_m^\dagger c_{km} \rangle = E_0 - \varepsilon_f. \tag{17b}$$

To calculate the expectation values in (17) we need to calculate propagators. In (17*a*) we need the f–f propagator $G_f(\varepsilon)$, described by the series in figure 8(*a*). We may in mean-field theory, essentially one-body theory, use retarded propagators. Summing from figure 8(*a*) we obtain

$$G_f(\varepsilon) = [\varepsilon - \varepsilon_f - F(\varepsilon)]^{-1}, \tag{18}$$

where the self-energy $F(\varepsilon)$ is ($s = 0^+$)

$$F(\varepsilon) = \sum_k \frac{zV^2}{\varepsilon - \varepsilon_k + is} \approx -i\pi V^2 \varrho, \tag{19}$$

and

$$\varrho = \sum_k \delta(\varepsilon - \varepsilon_k).$$

In (19) we make the usual assumption that the band of k-states is wide, so that the real part of F is effectively constant and only contributes an uninteresting shift which is ignored. Then defining

$$\Delta_0 = \pi V^2 \varrho, \quad \Delta = \pi z V^2 \varrho, \tag{20}$$

(18) becomes

$$G_f(\varepsilon) = 1/(\varepsilon - \varepsilon_f + i\Delta), \tag{21}$$

where the density of f-states, $\varrho_f = -\pi^{-1} G_f$, is then given by

$$\varrho_f(\varepsilon) = \frac{\pi^{-1}\Delta}{(\varepsilon - \varepsilon_f)^2 + \Delta^2}. \tag{22}$$

We see that Δ is the *renormalized lifetime broadening* of the f-level, which is shifted to ε_f, the renormalized f-level energy.

The expectation value $\langle n_f \rangle$ is now obtained from (22) as a Friedel-like expression

$$\langle n_f \rangle = \int_{-D}^{0} f(\varepsilon)\varrho_f(\varepsilon)\, d\varepsilon = \frac{N}{\pi} \tan^{-1}\left(\frac{\Delta}{\varepsilon_f}\right), \quad T = 0, \tag{23}$$

where $f(\varepsilon)$ is the Fermi function. Now we have seen that V is to be taken as of order $N^{-1/2}$. We shall see below that ε_f is O(1). Then Δ/ε_f is O($1/N$) and the arctangent may be expanded to give

$$\langle n_f \rangle \equiv n_f \sim N\Delta/\pi\varepsilon_f. \tag{24}$$

Since $0 < n_f < 1$, we see that Δ/ε_f is of order n_f/N. Thus because there are N channels in the quasiparticle resonance, its filling factor can only be small in order for n_f to be less than unity.

Hence we arrive at the picture of the density of f-states already illustrated in figure 6. The density of states is a Lorentzian centred on ε_f, of width 2Δ. Its filling factor is small: we illustrate the case $N = 6$, $n_f = 1$. In Yb systems the Lorentzian would be nearly filled in order to allow for ~ 1 hole; we recall that Yb systems are obtained by electron–hole inversion of Ce systems. The quantities Δ and ε_f are related by (24). Δ itself tends to be small, because of the renormalization factor $z = 1 - n_f$ in (20), especially when n_f lies very near to unity.

An explicit expression for the energy scale may be obtained from the other self-consistency relation (17*b*). The expectation value $\Sigma_k \langle f_m^\dagger c_{km} \rangle$ may be obtained from the f-conduction electron propagator G_{fc}, given by the series from figure 8 (*b*) as

$$G_{fc} = z^{1/2} V G_f G^0, \quad G^0(\varepsilon) = \sum_k \frac{1}{\varepsilon - \varepsilon_k + i s}, \tag{25}$$

so that

$$\sum_k \langle f_m^\dagger c_{km} \rangle = \frac{-z^{1/2} V}{\pi} \operatorname{Im} \int f(\varepsilon) G_f(\varepsilon) G^0(\varepsilon)\, d\varepsilon. \tag{26}$$

If we introduce the assumption that the conduction band consists of a constant density of states (DOS) ϱ above a lower band edge D,

$$\varrho(\varepsilon) = \varrho\theta(\varepsilon + D), \tag{27}$$

where $\theta(x)$ is the unit step function, then (26) becomes

$$\sum_k \langle f_m^\dagger c_{km} \rangle = \frac{-z^{1/2}\Delta_0}{\pi V} \operatorname{Im} \int_{-D}^{0} \frac{d\varepsilon}{\varepsilon - \varepsilon_f + i\Delta} f(\varepsilon) \tag{28}$$

$$= \frac{z^{1/2}\Delta_0}{2V\pi} \ln\left(\frac{\varepsilon_f^2 + \Delta^2}{D^2}\right), \quad T = 0. \tag{29}$$

In (28) we have used (19) and in (29) we assumed $D \gg \varepsilon_f$. Now inserting (29) into (17*b*) gives the equation for the energy scale

$$E_0 - \varepsilon_f = \frac{N\Delta^0}{\pi} \ln\left[\frac{(\varepsilon_f^2 + \Delta^2)^{1/2}}{D}\right]. \tag{30}$$

The equation (30) has an analytic solution for large negative E_0, the Kondo limit. Then we may drop ε_f from the left-hand side of (30), to get

$$(\varepsilon_f^2 + \Delta^2)^{1/2} \equiv T_K = D \exp(\pi E_0 / N\Delta_0). \tag{31}$$

The energy scale (31) can be very small as E_0 becomes large and negative. This is associated with n_f approaching unity and z thus approaching zero. The expression (31) indeed is correct in the large-N limit of the model (4), whose exact solution is known and whose energy scale may also be obtained by scaling arguments without involving the large-N approximation.

Note that the motivation for making V of order $N^{-1/2}$ is seen in (31). Such a choice makes the energy scale independent of N. We may define the energy scale to be T_K in the Kondo limit: in general, we may define the solution $(\varepsilon_f^2 + \Delta^2)^{1/2} \sim \varepsilon_f$ to (30) to be an energy scale T_A. Equations (23) and (30) may be combined into one by introducing [38] a single complex quantity $Z = \varepsilon_f + i\Delta$, which now obeys

$$Z_0 - Z = (N\Delta_0/\pi) \ln(Z/D), \tag{32}$$

where $Z_0 = E_0 + i\Delta_0$. T_A is then defined as $T_A \equiv |Z|$.

2.4. *Low-temperature thermodynamics*

Mean field is a non-interacting quasiparticle theory. The specific heat and susceptibility may be calculated using Sommerfeld theory. Since ε_f is small, $\varrho \ll \varrho_f$, and thus we may use the f-density of states as a reasonable approximation to the total density of states in most materials. Then we simply repeat the arguments of § 1.3, with ϱ_f now identified as the density of states (22) defined at the Fermi level $\varepsilon = 0$. Hence we obtain for γ and χ

$$\gamma = \tfrac{1}{3}k_B^2 N\varrho_f(0) \simeq \tfrac{1}{3}k_B^2 n_f/\varepsilon_f, \quad N \text{ large}, \tag{33}$$

$$\chi = \tfrac{1}{3}\mu_{eff}^2 N\varrho_f(0) \simeq \tfrac{1}{3}\mu_{eff}^2 n_f/\varepsilon_f, \quad N \text{ large}, \tag{34}$$

$$\simeq \tfrac{1}{3}\mu_{eff}^2 \frac{n_f^2}{1 - n_f}\frac{1}{N\Delta_0}, \quad N \text{ large}, \tag{35}$$

where

$$\mu_{eff}^2 = g^2\mu_B^2 j(j + 1) \tag{36}$$

is the effective moment of the RE atom in its degenerate configuration. It is seen that we get back (10) for the χ/γ ratio in mean field (MF)

$$\chi/\gamma = \mu_{eff}^2/(\pi^2 k_B^2). \tag{37}$$

We should now compare the MF results with the exact Bethe *ansatz* solutions. Considering first the Kondo limit $n_f = 1$, the results for χ and γ from Bethe *ansatz* are [24, 26]

$$Z = \mu_{eff}^2/(3T_\chi), \quad \gamma = \frac{k_B^2}{3}\frac{1}{T_\chi}\left(\frac{N - 1}{N}\right).$$

These results involve the characteristic energy scale T_χ. T_χ may be given by (31) (though in fact it depends on cut-off procedures introduced into the model). At large N, the expressions for χ, (12) and (34), can therefore be considered to be the same, since T_K tends to ε_f at large N.

The expression for γ cannot be identified with that of (33) by adjustment of T_χ, since the χ/γ ratio

$$\frac{\chi}{\gamma} = \frac{\mu_{eff}^2}{\pi^2 k_B^2}\left(1 + \frac{1}{N - 1}\right).$$

characteristically differs from (37) by a factor which can be as large as two for $N = 2$. However, it is only 15% for $N = 6$ and 12% for $N = 8$. In any case, the factor approaches one for N large. Thus all MF results do approach the exact solution as $N \to \infty$. For $n_f < 1$, $\chi(n_f)$ has been carefully investigated by Hewson and Rasul [36], and found to be in excellent agreement with the exact result, as illustrated in figure 9. The corrections to χ/γ also get smaller as n_f decreases [40, 49] (see § 9). Hence we conclude that for low temperatures and fields, the MF results are in good accord with exact solutions.

Looking now at correlations with experimental IV systems, we notice that it follows from (37) that mean-field theory explains the correlation in figure 2 which is observed empirically, if we could be satisfied with a treatment based on non-interacting impurities.

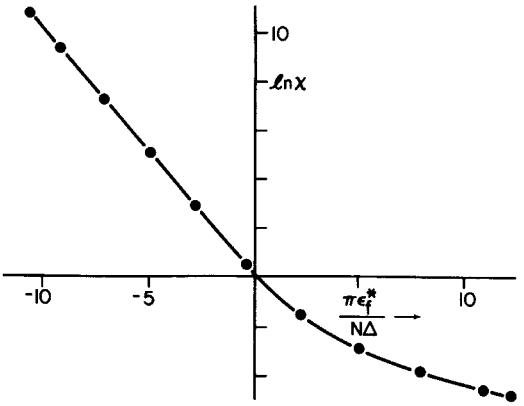

Figure 9. $T = 0$ magnetic susceptibility χ of 8-channel $U = \infty$, Anderson impurity model against scaled f-level energy ε_f^*. The full line is the Bethe *ansatz* [26] result, the points are from calculation to leading and next leading order in $1/N$ [36].

Table 2. Specific-heat linear coefficient γ, susceptibility χ and other parameters (see text for definition) for various compounds involving intermediate-valence species.

Compound	$\chi(0)$ (10^{-3} EMU mol^{-1})	γ (mJ mol^{-1} K^{-1})	R	$v_f(0)$	Δ (meV)	$\varepsilon_f - \varepsilon_F$ (meV)
YbCuAl	25·5	260·0	1·04	1·0	3·23	−7·8
$Y_{0.1}Yb_{0.9}CuAl$	27·5			1·0	3·0	−7·2
$YbCu_2Si_2$	16·0	135·0	1·26	1·0	6·4	−15·5
$YbAl_3$	4·7	45·0	1·07	1·0	17·7	−42·7
$YbAl_2$	0·41	16·8	0·25	1·0	52·0	−125·0
$CeSn_3$	1·46	53·0	0·94	0·9	18·9	37.0
$CePd_3$	1·47	37·0	1·36	0·9	18·9	37.0
αCe	0·51	12·8	1·36	0·3	8·6	54·0

Secondly, we illustrate in figure 5 the result of plotting equation (35) with $D_0 = 0{\cdot}19$ eV [40]. It is seen to fit quite well to the data (which we should remember involves considerable inaccuracy in determining n_f). These theoretical results (35) and (10) would in any case be very little different if we used the exact Bethe *ansatz* solutions rather than the MF results (33)–(35). It is interesting to see what values we get for D and ε_f if we fit χ (or γ) to experimental results for a representative sample of IV compounds [11]. This is done [11] in table 2, where we used (33), (34) and (22) without taking the $N \to \infty$ limit. We see that ε_f values for IV systems go down to ~ 8 meV for YbCuAl.

Another quantity which it is interesting to calculate is the charge susceptibility

$$\chi_C = \partial \langle n_f \rangle / \partial E_0.$$

This is done by recalculating the stationary point at a function of E_0, when we obtain in the large-N limit [40]

$$\chi_C = -n_f^2(1 - n_f)\pi/(N\Delta_0), \tag{38}$$

χ_C is seen to differ greatly from χ as given in (35). Whereas χ diverges in the Kondo limit $n_f \to 1$, χ_C becomes zero there. This is indeed a reasonable result, since in the

Kondo limit the f-level is reduced to a spin which does not change its occupation. χ_C against n_f is plotted on figure 5 (note scale factor); it is seen to be rather small.

It is interesting to obtain the ground-state energy E_g in mean field [40]. This is readily done starting from (40) below; if the arctangent is linearized (leading-N approximation) the integral performed and (30) used, we obtain in leading-N approximation

$$E_g = E_0 - \varepsilon_f. \tag{39}$$

2.5. *Higher temperatures and fields*

Now it is interesting to see what happens as we go away from the stationary point (ε_f, Δ), which is the solution to (32), obtained at zero temperature and zero field h. Let us add the Zeeman term (6) into the mean-field Hamiltonian (16). Then at finite temperature it is easy to derive the results

$$F = \frac{1}{\pi}\sum_m \int_{-D}^{D} d\varepsilon\, f(\varepsilon) \tan^{-1}\left(\frac{\Delta}{\varepsilon - \varepsilon_f + hm}\right) + (\varepsilon_f - E_0)\left(\frac{\Delta}{\Delta_0} - 1\right) \tag{40}$$

for the free energy, and the self-consistency equation (prime implies derivative)

$$-\sum_m \int_{-\infty}^{\infty} d\varepsilon\, \varepsilon f'(\varepsilon) \ln\left(\frac{Z - hm - \varepsilon}{\tau_K}\right) + \frac{\pi Z}{\Delta_0} = 0,$$

where

$$Z = \varepsilon_f + i\Delta, \quad \tau_K = D \exp\left[\frac{\pi}{N\Delta_0}(E_0 + i\Delta_0)\right].$$

To calculate, say, C_v to $O(T^3)$, first one sets $h = 0$ and expands Z to $O(T^2)$, obtaining (41 *a*, *b*). The result is substituted into (40) to get the Sommerfeld-like expansion for F, but this differs from the completely non-interacting problem because of the T-dependence of the mean field variables. Similarly, one may calculate χ and the moment M to $O(T^2)$ and $O(h^2)$ respectively.

The results are rather complicated in general, but in the large-N limit we obtain more simply [38, 40]

$$\varepsilon_f = T_A + \frac{\pi^2 T^2 n_f}{6T_A}, \tag{41 a}$$

$$\Delta = \Delta^0 + \frac{\pi^3 T^2 n_f}{6NT_A}(n_f - 2), \tag{41 b}$$

$$\chi(T) = \chi_0(1 + \kappa T^2) = \chi_0\left[1 + \frac{\pi^2 T^2}{30T_A^2}(5n_f^2 - 20n_f + 30)\right], \tag{41 c}$$

$$C_V(T) = \gamma T(1 + B_e T^2) = \gamma T\left[1 + \frac{\pi^2}{10}\frac{T^2}{T_A^2}(5n_f^2 - 20n_f + 42)\right], \tag{41 d}$$

$$M(h) = \chi_0 h(1 + \mu h^2) = \chi_0 h\left[1 + \frac{(hj)^2}{30T_A^2}(5n_f^2 - 20n_f + 18)\right] \tag{41 e}$$

$$n_f(T) = n_f(0)\left[1 + \frac{\pi^2}{6}\frac{T^2}{T_A^2}(1 - n_f)(2 - n_f)\right]. \tag{41 f}$$

Table 3. Comparison of expansion coefficients for mean-field large-N values, the exact Bethe *ansatz* results and experimental data on YbCuAl.

	κ	B_e	μ
Large-N	$\pi^2/2$	$2{\cdot}7\pi^2$	$j^2/10$
	4·93	27	1·2
Exact	$\simeq 5{\cdot}4$	$\simeq 35$	1·9
YbCuAl	>0	18	1·9

We see from (41 *a*, *b*) that ε_f increases with T, but Δ *decreases*. For all values of n_f, χ and γ have positive T^2 coefficients and $M(h)$ has a positive h^3 coefficient. This positiveness is typical of the large-N situation. If we consider the special case $n_f = 1$, without taking the $N \to \infty$ limit, all these coefficients turn out to be proportional to $\sin(3\pi/N)$, i.e. they are positive for $N > 3$. This result is actually found to be in agreement with exact solutions [22, 23]. As seen from figure 3, all the curves do turn upwards initially at the N-value $N = 8$, for which the figure 3 curves are calculated. But the exact solutions show that for $N < 3$ the curvature is negative.

In table 3 we illustrate the values of the χ, C_V and M coefficients obtained in the Kondo limit, $n_f = 1$, for $N = 8$. We see that the mean-field values are in fair agreement with the exact Bethe *ansatz* results for $N = 8$ [22, 23]. They are also in fair agreement with experimental data on YbCuAl [20, 21].

Equation (41 *e*) shows the correlation of n_f with T: n_f increases with T (up to $n_f = 1$ at $T \sim T_A$). In [11] we considered the variation of n_f with T of a number of experimental IV systems and showed it did indeed follow this sign in all cases. The variation of n_f occurs over a very narrow temperature range for YbCuAl (Mattens, Holscher, Tuin, Moleman and de Boer, preprint), which is to be expected as T_A is small for this material (table 2).

A qualitative discussion of the figure 4 trend of χ against $1/T_A$ is possible here. χ may be written from (34) in the large-N limit

$$\chi = \tfrac{1}{3}\mu_{\text{eff}}^2 n_f / T_A .$$

Hence for a moderate range of n_f (say 0·5 to 1), χ scales with T_A^{-1}, while from (41 *c*) we see that the temperature dependence scales as T/T_A (although the maximum is not determined at the T^2 level, the positive T^2 coefficient ensures the existence of a maximum in χ). Hence we can qualitatively understand the correlation in figure 4.

In order to explore higher temperature and fields than can be reached with the expansions (41), equations (39) and (40) can be treated numerically: in fact (40) was solved by a complex Newton–Raphson procedure and the result substituted in (39) (Newns, unpublished work).

We carried out computations in the Kondo limit $n_f = 1$, keeping $N = 8$ in the mean-field formulae. It is found that Δ, which decreases with T to $O(T^2)$ (41 *b*), *vanishes* at a critical temperature $\approx 0{\cdot}6T_K$. Results for $C_V(T)$, $\chi(T)$ and $M(h)$ are illustrated in figure 10. It is seen that while MF is very accurate for $T \leqslant 0{\cdot}25\,T_K$, because of this phase transition results at high temperature are very poor. A similar phase transition in h would be evident in figure 10 (*c*) were it carried to higher field. A similar comparison is given by Coleman [41] using his version of large-N theory.

In conclusion, for large-N mean field works excellently at low temperatures and fields, but fails disastrously at higher temperatures and fields. In this, mean field is in

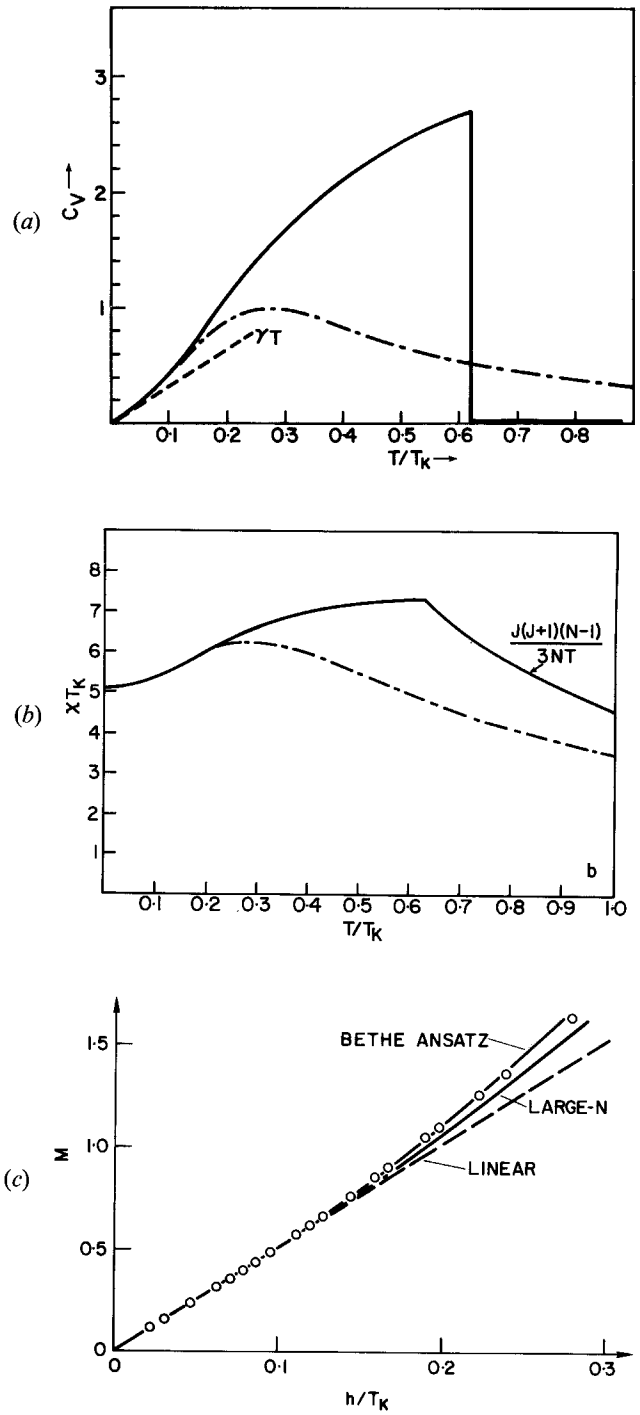

Figure 10. Plots of (*a*) Specific heat C_V in units of T_K against T; (*b*) magnetic susceptibility against T; and (*c*) magnetization against h, plots for the 8-channel, integral-valent $U = \infty$ Anderson model. The full curves are given by the mean-field solution. The exact solutions are the dot–dash curves [22] in (*a*), (*b*) and the upper full curve [23] in (*c*). In (*c*), the circles are experimental points [20].

interesting contrast to another approach, the non-crossing approach (NCA) [50], which sums all non-crossing diagrams in the Keiter–Kimball approach, but is not systematic in $1/N$. The NCA gives divergent results at very low temperatures, but correct results at high and intermediate temperatures [50, 51].

2.6. *Cut-offs and crystal fields*

Notice that (27) only contained the lower band cut-off D. If we introduce a square band with upper cut-off E so that a real part of G^0 is defined

$$G^0(\varepsilon) = -i\pi\varrho\theta(\varepsilon - D)\theta(E - \varepsilon) + \varrho \ln\left|\frac{\varepsilon + D}{\varepsilon - E}\right|, \tag{42}$$

then in the Kondo limit (31) becomes (Newns, unpublished work)

$$T_K = D^{1-1/N}E^{1/N}\exp(\pi E_0/N\Delta_0). \tag{43}$$

We see that the upper cut-off only appears as a $1/N$ effect, but at $N = 2$ its appearance restores electron–hole symmetry (though the prefactor in (43) is not exact for $N = 2$) [51, 52].

Crystal-field effects have been discussed by various authors, using exact Bethe *ansatz* procedures [53, 54] and within a large-N formulation [37]. The latter approach may be equivalently formulated in mean field. Suppose that the N levels are split into two subsets, a set at E_0 of degeneracy N_1 and a set at $E_0 + A$ of degeneracy N_2, where we assume $A > 0$. the splitting A now appears directly in ε_f in (16), and (30) generalizes to

$$E_0 - \varepsilon_f = \frac{\Delta^0}{\pi}\left(N_1 \ln\frac{\varepsilon_f}{D} + N_2 \ln\frac{\varepsilon_f + A}{D}\right). \tag{44}$$

The expression for T_K may be written down from (44) in the limit $A, (-E_0) \gg T_K$:

$$\varepsilon_f = T_K = T_K^0(T_K^0/A)^{N_2/N_1}, \tag{45}$$

Where T_K^0 is given by (31). Equation (45) is well known [37, 53, 54] and shows that although there is a reduction of the energy scale due to crystal fields, the reduction is by a power of (T_K^0/A).

3. Anderson SU(N) Dimer

3.1. *Model and mean field*

The case of two Anderson impurities 1 and 2 at a distance R apart in an electron gas has considerable importance as a first step in the lattice problem. This problem has been discussed by Jayaprakash *et al.* [55] and Lacroix *et al.* [56] for spin $\frac{1}{2}$ and by Coleman [42] and by Rasul (unpublished work) for the SU(N) case. Recently the spin-$\frac{1}{2}$ case has been treated by Wilson's [9] numerical renormalization group procedure [57]. The mean-field approach to the SU(N) case was carried out by Dharamvir (unpublished). In the SU(N) case let us start by introducing the Lagrange multipliers for the Q-constraints, when the Hamiltonian for two f-sites and 1 and 2 may be written, in an obvious notation

$$H = H_0 + E_0(n_{f1} + n_{f2}) + V\sum_{\mathbf{k},m}[f_{m1}^\dagger c_{\mathbf{k}m}b_1 + f_{m2}^\dagger c_{\mathbf{k}m}\exp(i\mathbf{k}\cdot\mathbf{R})\, b_2 + \text{h.c.}]$$
$$+ \gamma_1(b_1^\dagger b_1 + n_{f1} - 1) + \gamma_2(b_2^\dagger b_2 + n_{f2} - 1), \tag{46}$$

introducing two Lagrange multipliers γ_1 and γ_2. We now wish to make a mean-field approximation. To do this, the assumption is that *the symmetry of the model is retained,*

i.e. $\langle b_1 \rangle = \langle b_2 \rangle = z^{1/2}$, $\gamma_1 = \gamma_2 = \varepsilon_f - E_0$. The symmetry of the mean-field Hamiltonian lends itself to use of even and odd f-states $f_\pm = (f_1 \pm f_2)\sqrt{2}$, in terms of which the mean-field Hamiltonian H' becomes

$$H' = H_0 + \varepsilon_f(n_{f+} + n_{f-}) + z^{1/2} \sum_{\mathbf{k},m} (V_{\mathbf{k}+} f^\dagger_{+m} c_{\mathbf{k}m} + V_{\mathbf{k}-} f^\dagger_{-m} c_{\mathbf{k}m} + \text{h.c.}) + 2(\varepsilon_f - E_0)(z - 1), \tag{47}$$

where

$$V_{\mathbf{k}\pm} = (1/\sqrt{2})V(1 \pm \exp(i\mathbf{k} \cdot \mathbf{R})). \tag{48}$$

Now scatterings from + to − through $|k\rangle$ vanish, but we need the lifetime broadenings within the +, − channels

$$\Delta_\pm(\varepsilon) = -\frac{1}{i} \sum_{\mathbf{k}} |V_{\mathbf{k}\pm}|^2/(\varepsilon - \varepsilon_{\mathbf{k}} + is) = \Delta\left(1 \pm \frac{\sin kR}{kR}\right), \quad \varepsilon = k^2/2. \tag{49}$$

Writing down the self-consistency conditions, analogous to the single-impurity ones, for the large-N limit, at $T = 0$

$$2(1 - z) = n_{f+} + n_{f-} = \frac{N}{\pi} \int_{-D}^{0} \frac{d\varepsilon}{(\varepsilon - \varepsilon_f)^2} (\Delta_+ + \Delta_-), \tag{50}$$

or using (22)–(23),

$$1 - z = N\Delta/(\pi\varepsilon_f) = \tfrac{1}{2}(n_{f+} + n_{f-}), \tag{51}$$

we retrieve the same result as in the single-impurity case. The second relationship is

$$4(E_0 - \varepsilon_f) = \sum_{\mathbf{k},m} (V_{\mathbf{k}+} \langle f^\dagger_{+m} c_{\mathbf{k}m} \rangle + V_{\mathbf{k}-} \langle f^\dagger_{-m} c_{\mathbf{k}m} \rangle + \text{c.c.}, \tag{52}$$

or, to leading order in $1/N$,

$$4(E_0 - \varepsilon_f) \simeq \frac{2N}{\pi} \int_{-D}^{0} d\varepsilon \, (\Delta_+ + \Delta_-)/(\varepsilon - \varepsilon_f),$$

i.e. using (49)

$$(E_0 - \varepsilon_f) = (N\Delta^0/\pi) \ln(\varepsilon_f/D). \tag{53}$$

Again, the same equation is obtained as for the single-impurity case. At large distances, we see from (49) that both odd and even levels have the same width.

At small distances, $R \ll k_f^{-1}$, Δ_- is seen from (49) to become very small and the odd level is a narrow and unoccupied one lying above the Fermi level at ε_f. Then, assuming we are near the Kondo limit, $n_{f+} \sim 2$, $n_{f-} \sim 0$, so from (50) $\Delta_+ = 2\pi T_K/N = 2\Delta$. So we have the odd level with vanishing width, and the even level with twice the width of the single impurity resonance. The energy scale, however, remains T_K. We illustrate the density of states in the even and odd channels in figure 11.

3.2. *RKKY interaction*

It is necessary for understanding the properties of both the SU(N) dimer and lattice to estimate the RKKY interaction. This interaction is associated with the bare energy scale, and in the SU(N) dimer occurs when an electron occupies the same

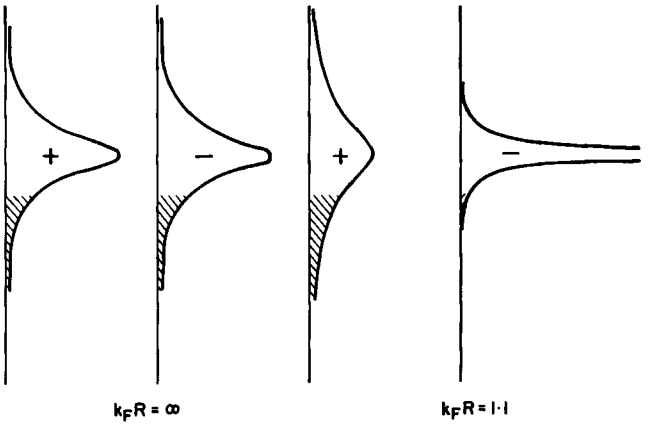

Figure 11. Sketch of f-density of states in even and odd channels (+, − respectively) for two RE impurities a distance R apart. Left hand two curves for $R = \infty$, right hand two curves for $k_F R = 1{\cdot}1$.

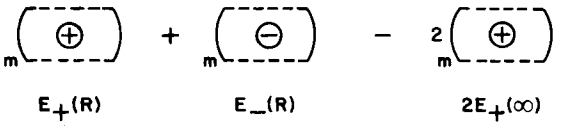

Figure 12. Diagrams for RKKY energy of two RE impurities at distance R apart, assuming mth channel occupied in both impurities. Full line, bare f-propagator, broken line, bare k-propagator, with parity + or − indicated on diagram. Vertex is $V_{k\pm}$.

m-state of each impurity. Since this situation does not violate the requirement that $0 < n_f < 1$ on each impurity, (a special situation arising because symmetry is broken) we can treat the problem as a one-body problem with the original (4*a*), without need of the P-operators.

The interaction energy E_{RKKY} is then given by the diagrams of figure 12. Using Feynman rules we have for the contribution from the even and odd channels E_+ and E_-

$$E_\pm(R) = \frac{V^4}{8E_0^2}\frac{1}{2\pi i}\sum_{\mathbf{k},\mathbf{k}'}\int d\omega \frac{g_\pm(\mathbf{k})g_\pm(-\mathbf{k})g_\pm(\mathbf{k}')g_\pm(-\mathbf{k}')}{(\omega - \varepsilon_k + i\delta \operatorname{sgn}\varepsilon_k)(\omega - \varepsilon_{k'} + i\delta \operatorname{sgn}\varepsilon_{k'})}. \quad (54)$$

where $g_\pm(\mathbf{k}) = 1 \pm \exp(i\mathbf{k}\cdot\mathbf{R})$. In (54) the propagator $(\omega - E_0)^{-1}$ has been trunctated to $-E_0^{-1}$, the RKKY interaction being calculated perturbationally, i.e. it applies when E_0 is large negative and we are near the Kondo limit. Now carrying out the ω-integral in (54) we obtain

$$E_{RKKY} = E_+(R) + E_-(R) - 2E_+(\infty),$$

as

$$E_{RKKY} = \frac{2J^2}{R^2}\int \frac{\varrho(\varepsilon_k)\,d\varepsilon_k}{k}\int \frac{\varrho(\varepsilon_{k'})\,d\varepsilon_{k'}}{k'} f_k(1 - f_{k'})\frac{\sin kR \sin k'R}{\varepsilon_k - \varepsilon_{k'}}, \quad (55)$$

J is defined as V^2/E_0 in § 1.2.

The usual case for which (55) is evaluated is for parabolic bands, $\varepsilon_k = k^2/2m^*$, $\varrho_k = (k/k_F)\varrho_F$, ($\varrho_F = \varrho(\varepsilon_F)$), whence

$$E_{\mathrm{RKKY}} = 8\pi(J\varrho_F)^2\varepsilon_F F(2k_F R)\delta_{mm'}, \tag{56}$$

where

$$F(x) = (x\cos x - \sin x)/x^4. \tag{57}$$

In (56) we have inserted $\delta_{mm'}$ since the interaction is zero unless $m = m'$.

3.3. *RKKY and mean field*

At this point we encounter a problem with mean field. The energy in mean field of two SU(N) impurities in the large-N limit will be, from the results of § 3.1., $2(E_0 - \varepsilon_f)$. The energy of two nearly-Kondo impurities if they break symmetry and go into a 'magnetically locked' state will be $\sim 2E_0 - E_{\mathrm{RKKY}}(R)$. In particular E_{RKKY} becomes attractive at small R, so what happens to the Kondo states if $E_{\mathrm{RKKY}} < -2\varepsilon_f$? Presumably the Kondo states are radically altered if R is smaller than the value satisfying [42]

$$\left.\begin{aligned} (k_F R)^3 &\lesssim C\,\frac{1}{N^2}\,\frac{(NJ\varrho_F)^2 D}{T_K} \\ \text{or} \qquad (k_F R)^3 &\lesssim C\,\frac{1}{N^2}\left(\frac{N\Delta_0}{\pi E_0}\right)^2\frac{D}{T_K}. \end{aligned}\right\} \tag{58}$$

In (58) we have explicitly displayed the N-dependence and kept all other quantities of order N^0. C is a constant of order unity.

We see that if we are in the $N \to \infty$ limit then R can be arbitrarily small without destroying the Kondo effect; the RKKY is an effect of rather high order in $1/N$. But because of the factor D/T_K, the right-hand side of (58) might still be large, at large but finite N. We discuss the problem more quantitatively in the next section.

Indeed the phenomenon of 'ferromagnetic locking' of the spins at small R occurs and has been discussed for SU(2) by Jayaprakash *et al.* [55]. They found that at small R a new Kondo energy scale T_K took over, corresponding to compensation by the host of the block spin formed of the two impurity spins ferromagnetically locked together. This work has been generalized by Dharamvir to the SU(N) case, and the situation found that the new energy scale took over precisely at an R given by (58) (Dharamvir, Read and Newns, unpublished work). Therefore, although formally an effect of high order in $1/N$, the RKKY energy can take over if T_K is too small because it involves unrenormalized quantities.

Very recently a numerical renormalization group calculation by Jones and Varma [57] for two spin-$\frac{1}{2}$ impurities has generated novel results not altogether in accord with conclusions based on the inequality (58) or the work of [55]. Jones and Varma conclude that, in the case where the RKKY coupling is ferromagnetic then the two impurity moments are coupled together *irrespective* of whether T_K is larger or smaller than the RKKY coupling. However, only a small correction to the temperature scale [57] is found, so the implications for heavy-fermion systems may ultimately be essentially of perspective.

4. The SU(N) Anderson lattice

4.1. *Mean-field solution*

The lattice of an IV compound such as $CeSn_3$ is a complex entity. We have s,p bands originating on the Sn and Ce sites, and 5d bands originating on the Ce sites, as well as the 4f band in which the strongest electron–electron interactions are occurring [43, 58]. This situation is one which can only be handled realistically by numerical band-structure programs and is not well adapted to the many-body type of theoretical approach.

Accordingly theorists introduce the SU(N) lattice model. In this model the f-states are described realistically, and a realistic feature of the spd band complex, its high degeneracy, is retained. But the 'host' spd bands are assumed to have the same N-fold degeneracy as the f-sites, and the mth host band is assumed to hybridize only with the mth impurity f-level. this model is an artificial extension of the conventional SU(2) spin concept to SU(N), its advantage being its comparative simplicity. The model is assumed, following the single-impurity model, to have $U = \infty$.

The SU(N) lattice model may accordingly be written [40, 42–45] in bosonized form

$$H = H_0 + E_0 \sum_i n_{fi} + V \sum_{im} (f_{im}^\dagger c_{im} b_i + \text{h.c.}), \tag{59a}$$

with the set of constraints

$$Q_i = n_{fi} + b_i^\dagger b_i = 1.$$

In (59), c_{im} is a localized conduction-band state on site i defined by

$$c_{im} = N_s^{-1/2} \sum_{\mathbf{k}} c_{\mathbf{k}m} \exp(i\mathbf{k} \cdot \mathbf{R}_i), \tag{59b}$$

where N_s = number of lattice sites. The specialized features of the SU(N) model are that we assume one atom per unit cell, we have hybridization only between the mth f-level and the mth conduction state (59b), and we shall assume that only one conduction band of k-states, where $\mathbf{k}$ lies in the Brillouin zone (BZ), is involved in the hybridization.

A mean-field approximation is introduced in which $\langle b_i^\dagger \rangle = \langle b_i \rangle = z^{1/2}$, where $\langle b_i \rangle$ is assumed site-independent to retain translational invariance. Similarly, the constraint is included by a term $(\varepsilon_f - E_0) \Sigma_i (n_{fi} + b_i^\dagger b_i - 1)$, again chosen to be translationally invariant. Then the mean-field Hamiltonian can be written [40, 42–45]

$$H' = \sum_{\mathbf{k},m} \varepsilon_k n_{\mathbf{k}m} + \sum_i \varepsilon_f n_{fi} + z^{1/2} V \sum_{i,m} (f_{im}^\dagger c_{im} + \text{h.c.}) + (\varepsilon_f - E_0)(z - 1) \sum_i 1, \tag{60a}$$

or in k-space as

$$H' = \sum_{\mathbf{k},m} [\varepsilon_k n_{\mathbf{k}m} + \varepsilon_f f_{\mathbf{k}m}^\dagger f_{\mathbf{k}m} + z^{1/2} V (f_{\mathbf{k}m}^\dagger c_{\mathbf{k}m} + \text{h.c.}) + (\varepsilon_f - E_0)(z - 1)], \tag{60b}$$

where

$$f_{\mathbf{k}} = N_s^{-1/2} \sum_i f_i^\dagger \exp(i\mathbf{k} \cdot \mathbf{R}_i).$$

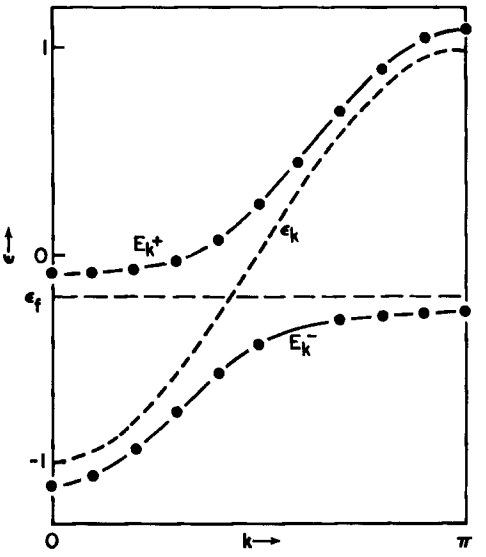

Figure 13. Renormalized band structure of a heavy-fermion system along one direction in k space for a particular m value. The assumptions made are that $\varepsilon_k = \cos k$, $\varepsilon_f = -0{\cdot}2$ and $zV^2 = 0{\cdot}1$.

Equation (60 *b*) describes a renormalized band-structure problem in which the renormalized f-level ε_f hybridizes through the renormalized matrix element $z^{1/2}V$ with the k bands, conserving m (see figure 13). The energy bands are [41, 42–45]

$$E_k^{\pm} = \tfrac{1}{2}\{\varepsilon_f + \varepsilon_k \pm [(\varepsilon_f - \varepsilon_k)^2 + 4zV^2]^{1/2}\}.$$

However, for many purposes, such as the self-consistency equations, it is more convenient to work with propagators.

The self-consistency equations are obtained by differentiating (60) with respect to ε_f and $z^{1/2}$

$$1 - \langle n_f \rangle = z, \tag{61 a}$$

$$V \operatorname{Re} \sum_m \langle f_{im}^\dagger c_{im} \rangle = E_0 - \varepsilon_f. \tag{61 b}$$

The calculation of (61) may be done by introducing the retarded Green functions for the system. This follows closely the work of Lacroix and Cyrot [31]. We introduce the conduction-band propagators per channel

$$G_c(\omega) = N_s^{-1} \sum_k \left(\omega + is - \varepsilon_k - \frac{zV^2}{\omega - \varepsilon_f + is} \right)^{-1}, \tag{62 a}$$

a result following straightforwardly from (60 *b*). Also we introduce the f-propagator

$$G_f(\omega) = \frac{zV^2}{(\omega - \varepsilon_f + is)^2} G_c(\omega) + \frac{1}{\omega - \varepsilon_f + is}. \tag{62 b}$$

Now since the unperturbed conduction-band density of states per channel is

$$\varrho_0(\omega) = -\frac{\operatorname{Im}}{\pi N_s} \sum_k (\omega - \varepsilon_k + is)^{-1}, \tag{63}$$

the perturbed DOS $\varrho_c = -\pi^{-1} \operatorname{Im} G_c(\omega)$ is given by (per channel)

$$\varrho_c(\omega) = \varrho_0[\omega - (zV^2/\omega - \varepsilon_f)]. \tag{64}$$

Similarly, the DOS in the f-subspace is given by

$$\varrho_f(\omega) = \frac{V^2 z}{(\omega - \varepsilon_f)^2} \varrho_0\left(\omega - \frac{zV^2}{\omega - \varepsilon_f}\right). \tag{65}$$

Suppose we specialize to a rectangular form for the density of states ϱ_0

$$\varrho_0(\omega) = (2D)^{-1}\Theta(\omega + D)\Theta(D - \omega), \tag{66}$$

where $\Theta(\omega)$ is the step function, then (64) and (65) become

$$\varrho_c(\omega) = (2D)^{-1}[\Theta(\omega - \varepsilon_a)\Theta(\varepsilon_b - \omega) + \Theta(\omega - \varepsilon_c)\Theta(\varepsilon_d - \omega)] \tag{67}$$

and

$$\varrho_f(\omega) = \frac{V^2 z}{2D(\omega - \varepsilon_f)^2}[\Theta(\omega - \varepsilon_a)\Theta(\varepsilon_b - \omega) + \Theta(\omega - \varepsilon_c)\Theta(\varepsilon_d - \omega)]. \tag{68}$$

In equation (68) we have introduced the band edges $\varepsilon_a \ldots \varepsilon_d$, which are seen from (64) to be given by

$$\omega - (V^2 z/\omega - \varepsilon_f) = \pm D, \tag{69}$$

and take the values, in ascending order

$$\left.\begin{aligned} \varepsilon_a &= \tfrac{1}{2}\{\varepsilon_f - D - [(\varepsilon_f + D)^2 + 4zV^2]^{1/2}\} \\ \varepsilon_b &= \tfrac{1}{2}\{\varepsilon_f + D - [(\varepsilon_f - D)^2 + 4zV^2]^{1/2}\} \\ \varepsilon_c &= \tfrac{1}{2}\{\varepsilon_f - D + [(\varepsilon_f + D)^2 + 4zV^2]^{1/2}\} \\ \varepsilon_d &= \tfrac{1}{2}\{\varepsilon_f + D + [(\varepsilon_f - D)^2 + 4zV^2]^{1/2}\} \end{aligned}\right\} \tag{70}$$

The densities of states ϱ_c and ϱ_f are illustrated in figure 14. Notice the enhancement near ε_f in ϱ_f, which however has been chosen to be modest, for clarity of illustration.

To the self-consistency equations derived from minimizing the ground-state energy with respect to ε_f and z we need also to add a condition from varying chemical potential μ in order to fix the number of particles correctly. From the Hellman–Feynman theorem, we obtain by varying ε_f

$$n_f = 1 - z,$$

where, from (68),

$$n_f = N\frac{V^2 z}{2D}\int_{\varepsilon_a}^{\mu} \frac{d\omega}{(\omega - \varepsilon_f)^2} = \frac{NV^2 z}{2D}\left(\frac{1}{\varepsilon_f - \mu} - \frac{1}{\varepsilon_f - \varepsilon_a}\right). \tag{71}$$

By varying μ we get a condition for conservation of the total number of electrons n

$$n = n_f + N(\mu - \varepsilon_a)/2D. \tag{72}$$

By varying z we obtain

$$NVz^{-1/2}\langle f_{im}^{\dagger} c_{im}\rangle = E_0 - \varepsilon_f. \tag{73}$$

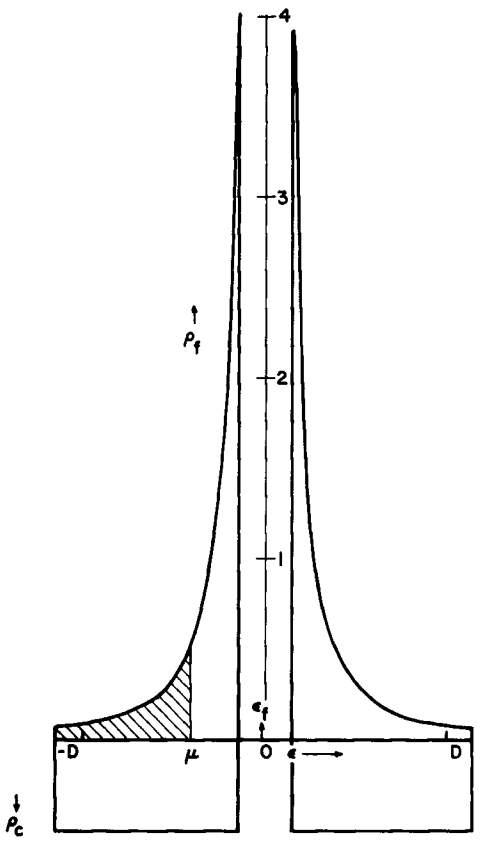

Figure 14. Density of states of SU(6) metallic heavy-fermion systems, f-DOS above abscissa, from equation (68), conduction-DOS below abscissa, from equation (67). Parameters are: unperturbed conduction band has rectangular DOS between $-D$ and D, $D = 1$, $n = 3$, $V^2 = 0{\cdot}825$, $E_0 = -2{\cdot}595$, $n_f = 0{\cdot}8$. Renormalized parameters calculated self-consistently from (71)–(74).

Here $\langle f^\dagger_{im} c_{im} \rangle$ may be obtained from $G_{fc} = z^{1/2} V G^0_f G_c = z^{1/2} V(\omega - \varepsilon_f)^{-1} G_c$, whence from (67)

$$E_0 - \varepsilon_f = \frac{NV^2}{2D} \int_{\varepsilon_a}^{\mu} d\varepsilon \, (\varepsilon - \varepsilon_f)^{-1} = NV^2(2D)^{-1} \ln [(\varepsilon_f - \mu)/(\varepsilon_f - \varepsilon_a)]. \quad (74)$$

4.2. *The 'metallic' case*

In this subsection we consider the typical metallic case [40], where the total number of electrons $n = n_c + n_f$ is of order $N/2$. The band edges may then be approximated by

$$\left.\begin{aligned} \varepsilon_a &\simeq -D - V^2 z/(\varepsilon_f + D), \\ \varepsilon_b &\simeq \varepsilon_f + V^2 z/(\varepsilon_f - D), \\ \varepsilon_c &\simeq \varepsilon_f + V^2 z/(\varepsilon_f + D), \\ \varepsilon_d &\simeq D - V^2 z/(\varepsilon_f - D). \end{aligned}\right\} \quad (75)$$

Introducing the familiar notations

$$\left.\begin{aligned} T_A &= \varepsilon_f - \mu, \quad \tilde{E}_0 = E_0 - \mu, \\ \Delta_0 &= \pi V^2/2D, \quad \Delta = \pi V^2 z/2D, \end{aligned}\right\} \tag{76}$$

(71)–(74) may be written [40]

$$\left.\begin{aligned} n_f &= N\pi^{-1}\Delta/T_A = 1 - \Delta/\Delta_0, \\ n_f &+ N(\mu + D)/2D = n, \\ -(N\Delta_0/\pi) &\ln [T_A/(D + \mu)] = T_A - \tilde{E}_0. \end{aligned}\right\} \tag{77}$$

From (77) we deduce, at $T = 0$

$$n_f = (1 + \pi T_A/N\Delta_0)^{-1}.$$

The results (77) are similar to those for a single impurity [40, 42, 43]. In figure 14 we have solved (71), (72) and (74) and plotted the DOS and position of μ for a typical metallic case with $n = 3$, $N = 6$ (for remaining parameters see figure caption). We have chosen a case with T_A very large ($\simeq 0{\cdot}4D$) for convenience in plotting, so $\varrho_f(\varepsilon_F)$ is not very large, but the qualitative features are clear.

The susceptibility and specific heat may be obtained from the density of states at the Fermi level [40]

$$\left.\begin{aligned} \chi_0 &= \frac{1}{3\mu_{\text{eff}}^2}\left(\frac{N}{2D} + \frac{n_f}{T_A}\right), \\ \gamma &= \frac{\pi^2 k_B^2}{3}\left(\frac{N}{2D} + \frac{n_f}{T_A}\right). \end{aligned}\right\} \tag{78}$$

Here we have included in calculating χ a coupling of h to conduction electrons with the same g factor as for f-electrons. These results are seen to be the same as for the single impurity equations (33) and (36), to leading order in $1/N$, provided the small contribution from the conduction electrons is neglected.

The charge response is found to differ from that for a single impurity, the charge susceptibility being given by [40]

$$\chi_c = \frac{dn_f}{dE_0} = \frac{-n_f^2(1 - n_f)\pi/N\Delta_0}{1 + n_f^2(1 - n_f)^2\pi D/N^2\Delta_0}. \tag{79}$$

This result is of order $-N/2D$, the charge response for the conduction electrons, unless the f-occupation is exceedingly close to 0 or 1. This is very small relative to χ_0 because $2D \gg T_A$. The reason for the appearance of the conduction-band density of states, is that if we raise the f-level E_0, $-\delta n_f$ electrons flow into the conduction band and raise μ there by $\delta\mu_c \sim \delta n_f N/2D$. This greatly exceeds the small decrease $\delta\mu_f' \sim -\delta n_f/T_A$ of μ in the f band. Hence is it the 'negative feedback' associated with the low conduction-band density of states which controls χ_c.

This much discussed difference between the lattice and sample impurity probably does not exist, or is greatly reduced, in real systems [18] due to interactions not present in the simplified Anderson lattice model. In such systems the lost δn_f electrons from an f-site reappear in the local screening cloud in the conduction band around the site (Friedel sum rule). At a distance of about $\sim 1{\cdot}5$ Å away from the site a negligible effect of δn_f on the conduction electrons is seen and there is no μ-shift. Since this is the

typical distance between 4f sites in IV materials, we expect the negative feedback effect to be negligible or greatly reduced. That this is actually true is seen by the measurable changes of valence in materials such as YbCuAl or $CeSn_3$ [59] with a change in T from 0 to $\simeq T_A$. This is just what would be expected from the impurity formula (41f). If negative feedback were operating, enormous temperatures of order $2D/N$ would be needed to generate an equivalent change in valence.

Thus we see that when N is large little difference between the SU(N) lattices in the metallic case and the single-impurity case has emerged so far, though the eigenstates, being of Bloch type are very different.

4.3. *Power series for G_f*

Another technique for examining the large-N behaviour of the lattice is to expand the propagators, e.g. G_f, in powers of V:

$$G_f(\varepsilon) = N_s^{-1} \sum_{\mathbf{k}} \{g_f^0(\varepsilon) + g_f^0(\varepsilon) z V^2 g_k^0(\varepsilon) g_f^0(\varepsilon) + g_f^0(\varepsilon)[z V^2 g_k^0(\varepsilon) g_f^0(\varepsilon)]^2 + \ldots\} \tag{80a}$$

where $g_f^0(\varepsilon) = (\varepsilon - \varepsilon_f + is)^{-1}$ and $g_k^0 = (\varepsilon - \varepsilon_k + is)^{-1}$. Now since V^2 is defined to be of order $1/N$ (see discussion following equation (27)), the terms in (80) form a $1/N$ expansion. The first makes no contribution to the DOS, so selecting only the second we have to leading order in N^{-1}

$$\varrho_f(\varepsilon) \simeq \varrho_0(\varepsilon) z V^2/(\varepsilon - \varepsilon_f)^2, \tag{80b}$$

which shows that the corrections in principle coming from the argument of ϱ_0 in (65) are of higher order in $1/N$. A similar result is found for other propagators and this will carry over into the self-consistency relations (71)–(74). Hence the use of the expansion (80) provides an alternative demonstration that the self-consistency relations and thermodynamic properties are impurity-like.

4.4. *The insulating case: $n = N$*

An interesting feature of the SU(N) lattice is that it seems to conceptually describe the insulating case of IV systems [41, 43]. In the case where the total number of electrons per RE site $n = N$, we have exact filling of the lower band between ε_a and ε_b, and hence an insulator (figure 14). By juggling with (71) and (75) (first and third equations) plus (69), we obtain for the band edges relative to ε_f (here $0 \leqslant n_f \leqslant 1$)

$$\left.\begin{aligned} \varepsilon_a &= \varepsilon_f - 2D[1 - n_f/N] + O(T_A), \\ \varepsilon_b &= \varepsilon_f - T_A, \\ \varepsilon_c &= \varepsilon_f + T_A n_f/(N - n_f), \\ \varepsilon_d &= \varepsilon_f + 2Dn_f/N + O(T_A). \end{aligned}\right\} \tag{81}$$

In (81) the third equation defines T_A. From (74), the energy scale T_A is given by

$$T_A = 2D\left(1 - \frac{n_f}{N}\right) \exp\left[\frac{(E_0 - \mu)\pi}{N\Delta_0}\right], \tag{82}$$

where Δ_0 is defined in (76).

In figure 15 we have sketched the solution to the self-consistency equations (71)–(74) for $N = n = 6$, $n_f = 5{\cdot}25$. This is the electron–hole inverse of the situation just described. Figure 15 qualitatively resembles SmS. The bands split into what is

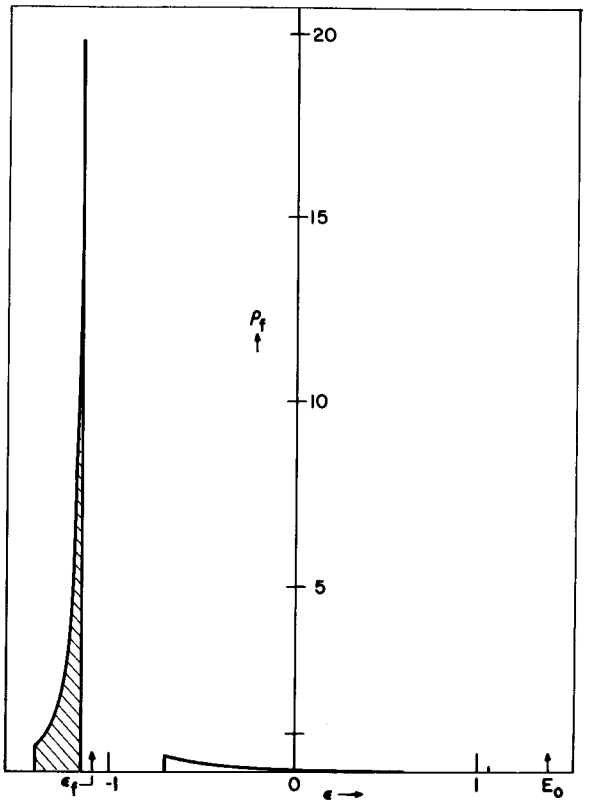

Figure 15. Density of states of SU(6) model for gold-SmS type of heavy-fermion system (only f-DOS illustrated). Calculation as for figure 14, with $n = 6$, $V^2 = 0{\cdot}492$, $E_0 = 1{\cdot}39$, $n_f = 5{\cdot}25$.

close to a description of a narrow filled f-band separated by a gap from a wider 'host' band (in SmS it is the Sm d-band). Figure 14 nevertheless qualitatively describes gold SmS; E_0 is above the 'host' band, and $\langle n_f \rangle$ is closer to 5 than 6, implying considerable fd mixing. In black SmS, presumably E_0 is below $-D$, giving an exceedingly narrow f-band with $\langle n_f \rangle$ close to 6.

In figure 16, we illustrate a version of the phase transition in SmS within the SU(N) model. Black SmS (upper portion) has n_f very close to 6, because E_0 is below $-D$. It has an exceedingly narrow f-band separated by a wide gap from the conduction band of the host. In gold SmS (lower portion) there will be some increase in V as a result of the volume contraction (we allowed only for a slight increase), but mainly E_0 is pushed into the 'host' band. Now we have a very-narrow-gap insulator, the f-band being relatively wide.

According to (81) the gap is of order $T_A N/(N - n_f)$ i.e. $\sim T_A$ (with electron–hole inversion the gap is $T_A N/n_f$). Hence in gold SmS we may speak of a 'Kondo' or many-body gap. The latter expression is more accurate, because in SmS the z-factor is only $\sim 1/4$, and most of the heavy mass really comes from a reduction in V due to the effect of projecting the hopping matrix elements [60] between the ground states of f^5 and f^6.

We should note that somewhat different discussions of SmS within the quasi-particle formulation have been given. Martin [61] considers strongly crystal-field split

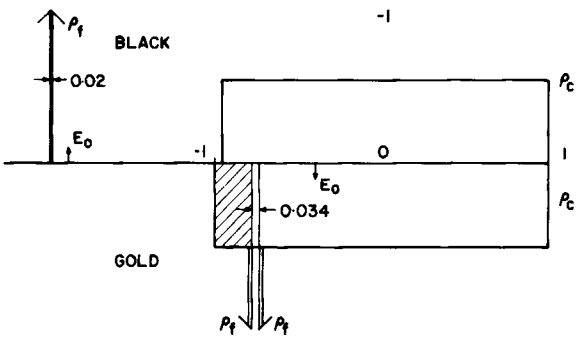

Figure 16. Comparison of black- and gold-type SmS in SU(6) model with $n = 6$. The conduction band DOS ϱ_c is illustrated. The f-DOS is too narrowly peaked to be plotted, and is replaced by arrows. Parameters are $E_0 = -1{\cdot}88$, $V^2 = 0{\cdot}0264$ in the black case, resulting in $n_f = 5{\cdot}95$ ($Sm^{2{\cdot}05+}$); $E_0 = -1{\cdot}40$, $V^2 = 0{\cdot}0305$ in the gold case, resulting in $n_f = 5{\cdot}25$ ($Sm^{2{\cdot}75+}$).

Sm levels interacting with realistic SmS d-bands. Read and Newns consider [43] SU(6) (non-crystal-field split) f-levels hybridizing with the realistic SmS d-bands, following [62] an early suggestion of Anderson that some of the f-bands are unhybridized, so that the gap will be between ε_f and the lowest point of the hybrid conduction band.

4.5. *RKKY interaction: stability towards magnetic ordering*

Those IV systems having n_f exceedingly close to one develop a very low energy scale $T_K \sim N\Delta_0(1 - n_f)$. Of course, they have accordingly huge susceptibilities and specific heats since these qualities are of order $1/T_K$. A refinement is that T_K may be lower than the crystal-field splitting, when the energy scale may be estimated from the expression (45). These $n_f \to 1$, high-susceptibility and specific-heat materials are termed Kondo lattices (sometimes overlapping 'heavy-fermion' materials, though the latter class is more general).

Another characteristic energy of the lattice is the magnetic interaction between spins on different sites which originates in the RKKY interaction (see § 3.2.). This interaction does not vary so critically when $n_f \to 1$ as the T_K energy scale. Therefore as $n_f \to 1$ the magnetic energy will exceed the 'kinetic energy' $\sim T_K$ of the lattice, leading to the onset of magnetic order. In fact there has been a question raised in the literature [42, 63, 64] as to how Kondo-lattice/IV materials can be stable against ordering, due to the smallness of T_K or T_A in these materials. In this section we shall address this problem briefly, and show by order-of-magnitude estimates that at least within the SU(N) model the boundary of the Kondo-lattice region is extensive enough to explain the experimental data. Part of the answer is that for N large, the leading-N energy T_K dominates over the RKKY interaction which is a higher-order effect (§ 3.2) in $1/N$.

The RKKY interaction [71] between two f-sites in the SU(N) lattice a distance R apart is given in the case of a parabolic band $\varepsilon_k = k^2/2m^*$ by (56):

$$E_{\text{int}}(m, m') = \delta_{mm'}(8\pi/N^2)(J_0\varrho_F)^2\varepsilon_F F(2k_F R), \tag{83}$$

where the RKKY interaction is

$$F(x) = (x\cos x - \sin x)/x^4,$$

and ϱ_F is the DOS of the conduction band at ε_F. J_0 is given by

$$J_0 = NV^2/|E_0|, \tag{84}$$

and (83) is only valid when E_0 lies well below ε_F. Notice that in (84) we have defined J_0 as of order one by introducing the factor N, V being defined to be of order $N^{-1/2}$. Hence E_{int} is formally of order N^{-2}.

The RKKY interaction is responsible for magnetism in RE metals, in whose magnetic state site occupations have a definite value of m constituting a superlattice [8]. This state contrasts with the normal Fermi-liquid ground state discussed above, where m-values are equally occupied on all sites (no symmetry breaking). The normal Fermi liquid and magnetic states will, in three dimensions, be separated by a *phase boundary*. As indicated above, a rough estimate of the condition for magnetism, along the lines of Jullien and Doniach [63] and Read, Newns and Doniach [42] is to compare the magnetic energy with the energy of the normal Fermi-liquid (FL) state. In the large-N limit we may use the value for one impurity for this energy. The condition for stability of the normal FL ground state against magnetism is then, if $D' = \mu + D$, essentially as we discussed in § 3.3

$$T_{\text{A}} = D' \exp(-1/\varrho_F J_0) \gtrsim (8\pi Z/2N^2)(J_0\varrho_F)^2 D' F(2k_F\bar{R}), \tag{85}$$

where Z is the number of nearest neighbours of a given site with the same m-value as the site, and $\bar{R}$ an average distance to such near neighbours. Calculations on simple models (unpublished) suggest that this is adequate as an estimate of the energy of the magnetic lattice. Notice that in the large-N limit the normal FL state is stable. In fact the condition (85) is satisfied if

$$T_{\text{A}}/D' > C/(2N \ln N)^2, \tag{86}$$

where

$$C = 4\pi Z F(2k_F\bar{R}). \tag{87}$$

This shows that two factors favour stability of the normal FL state: N being large and $2k_F\bar{R}$ being large. This goes some way to explaining the existence of normal 'Kondo-lattice' Fermi liquids in nature with remarkably low T_{A}. Thus supppose $Z = 8$, $N = 6$ and $k_F\bar{R} = 2\pi$ (a reasonably conservative choice), then with $D' = 2\,\text{eV}$ (86) gives

$$T_{\text{A}} > 2\,\text{K}, \tag{88}$$

quite a low limit on T_{A}.

Now the type of Kondo-lattice systems which lie near the phase boundary, e.g. $CeAl_3$, [4, 66] have low T_{A}, and the T_{A} values are normally less than the crystal-field splitting A, which as we have seen (equation (32)) in the case of splitting into an N_1-degenerate ground-state manifold leads to a new energy scale

$$T_{\text{A}}^{\text{c}} = T_{\text{A}}(T_{\text{A}}/A)^{N_2/N_1},$$

where $N_2 = N - N_1$. If we assume that crystal fields do not alter the RKKY interaction, then T_{A} replaces T_A in (85) and we can write (86) in terms of T_{A}^{c} instead of T_{A}:

$$T_{\text{A}}^{\text{c}}/D > C/(2N \ln N)^2. \tag{89}$$

Hence provided the energy scale including crystal-field splitting satisfied an inequality of order (89), the Kondo lattice will be non-magnetic as pointed out earlier [64]. This is indeed possible because the T_A^cs are not so low, the $(T_A/A)^{N_2/N_1}$ factor being only an order of magnitude or so.

Thus to summarize this section, Kondo lattices such as $CeAl_3$ are believed to lie near the magnetic phase-transition boundary, as shown for example by the fact that $CeAl_2$ is [1–4] magnetic. We can understand their stability by the fact that their T_As (or rather T_A^cs) lie above the critical value for that particular lattice. However, the critical value is quite low because of the largeness of N and because of the large RE–RE distances.

The condition for magnetic instability is similar to the condition (58) in the two-impurity problem for the moment to lock together and form a new low-energy scale. The difference from the bulk problem is here, of course, due to the lack of a phase transition in zero space dimensions.

4.6. *Comparison with other approaches*

There is no exact solution available for the SU(N) lattice as there is for the SU(N) $U = \infty$ impurity problem. Variational treatments [67–70] are available which provide some basis for comparison (also Oguchi, preprint). These treatments, based on the original Gutzwiller variational treatment of the Hubbard model [70], are essentially zero-temperature techniques though some extension to higher temperature has been made [68]. These treatments also generate a renormalization factor z of the f-conduction-band hopping-matrix element, which in Brandow's approach [67] is $z = 1 - n_f$, as in mean field. However, in the Ueda–Rice approach ([68], also Oguchi, preprint) a slightly different result,

$$z = (1 - n_f)/(1 - n_f/N),$$

is obtained. This leads to a correction to the exponent of the Kondo temperature (31, 76). Fazekas [69] applied the variational approach to a lattice with a concentration c of RE impurities, and showed that the renormalization factor z becomes $z = c(1 - n_f)/(1 - cn_f/N)$, while the Kondo exponential becomes

$$\exp\left[\frac{E_0}{V^2 N}\left(1 - \frac{c}{N}\right)\right].$$

Now mean field, being a leading-N result, is compatible with all these results. However, we notice that Fazekas' corrected energy scale resembles that of Jones and Varma [57] in the two-impurity problem if we identify c with (inter-impurity distance)$^{-3}$, which corroborates the results of Fazekas and [68].

A completely different approach (to the spin-$\frac{1}{2}$ lattice) was formulated by Yoshimori and Kasai [71], whose chief assumption was the locality in space of the f-electron self-energy. With this assumption, a calculation of many properties including very plausible results for the resistivity was possible.

A set of very useful Fermi-liquid relations, leading to conclusions on the χ/γ ratio and resistivity, for example, has been obtained by Yamada *et al.* [7], whose work is discussed in § 9.

5. Free-electron Anderson lattice

Another model, differing from the SU(N) lattice model, which is sometimes thought to provide a useful model of IV systems [60], is the free-electron Anderson

lattice in which the conduction bands are plane waves. Assuming one RE atom per unit cell i, with orbital angular momentum l', the model may be written in the same way as (59), except now H_0 is written in terms of the plane waves $|\mathbf{k} + \mathbf{g}, \sigma\rangle$

$$H_0 = \sum_{\mathbf{k},\mathbf{g},\sigma} \varepsilon_{\mathbf{k}+\mathbf{g}} n_{\mathbf{k}+\mathbf{g},\sigma}, \tag{90}$$

where $\mathbf{k}$ is a Bloch-wave vector inside the first BZ, and $|\mathbf{k} + \mathbf{g}\rangle$, of energy $\varepsilon_{\mathbf{k}+\mathbf{g}} = \frac{1}{2}|k + g|^2$, is a plane-wave state belonging to reciprocal-lattice vector $\mathbf{g}$, and spin $\sigma = \pm 1/2$. The interaction part of the Hamiltonian in (59) is written using a redefined localized conduction-band state c_{im}

$$c_{im} = \sum_{\mathbf{k},\mathbf{g},\sigma} (4\pi N_s)^{1/2} Y_{lm-\sigma}(\Omega_{\mathbf{k}+\mathbf{g}}) a_{lm\sigma} c_{\mathbf{k}+\mathbf{g},\sigma} \exp[\mathrm{i}(\mathbf{k} + \mathbf{g}) \cdot \mathbf{R}_i], \tag{91}$$

where $Y_{l\mu}(\Omega)$ is a spherical harmonic and the $a_{lm\sigma} = \langle |l, m - \sigma, \sigma | jm\rangle$ are CG coefficients; j is assumed to be 5/2 or 7/2. The volume of the lattice is v, assuming box normalization of the plane waves. The matrix element V is

$$V = \left(\frac{4\pi}{v}\right)^{1/2} \int_0^\infty r^2 \, \mathrm{d}r \, f(r) V(r) j_l(kr), \tag{92}$$

where $f(r)$ is the radial f-function and $j_l(\varrho)$ the order-l spherical Bessel function.

Suppose we now make the mean-field approximation, the effective single-particle Hamiltonian may again be written as (60), with the modifications (90)–(92). For simplicity in further considerations, let us confine ourselves to a spinless model in which $N = 2l + 1$; spin in any case may be regarded as a $1/N$ effect. The mean-field Hamiltonian is

$$H' = \sum_{\mathbf{k},\mathbf{g}} \varepsilon_{\mathbf{k}+\mathbf{g}} n_{\mathbf{k}+\mathbf{g}} + \sum_{i,m} \varepsilon_{\mathrm{f}} n_{im} + Vz^{1/2} \sum_{i,m} (f_{im}^\dagger c_{im} + \mathrm{h.c.}) + (\varepsilon_{\mathrm{f}} - E_0)(z - 1) \sum_i 1, \tag{93}$$

where

$$c_{im} = \sum_{\mathbf{k},\mathbf{g}} (4\pi N_s)^{1/2} Y_{l,m}(\Omega_{\mathbf{k}+\mathbf{g}}) c_{\mathbf{k}+\mathbf{g}} \exp[\mathrm{i}(\mathbf{k} + \mathbf{g}) \cdot \mathbf{R}_i]. \tag{94}$$

An approach to trying to calculate the propagators, which now become matrices in m and m', is through a series expansion such as (80). In the present case the series expansion for the trace of G_{f} starts off as (dropping the trivial term $(\varepsilon - \varepsilon_{\mathrm{f}})^{-1}$)

$$\mathrm{Tr}\,(G_{\mathrm{f}} - G_{\mathrm{f}}^0) = \sum_{\mathbf{k},\mathbf{g}} \frac{V^2 N N_s}{(\varepsilon - \varepsilon_{\mathrm{f}})^2 (\varepsilon - \varepsilon_{\mathbf{k}+\mathbf{g}} + \mathrm{i}s)} + \sum_{\mathbf{k},\mathbf{g},\mathbf{g}'} \frac{V^4 N^2 N_s^2}{(\varepsilon - \varepsilon_{\mathrm{f}})^3} P_l(\theta_{\mathbf{g}\mathbf{g}'}) \frac{1}{(\varepsilon - \varepsilon_{\mathbf{k}+\mathbf{g}'} + \mathrm{i}s)} P_l(\theta_{\mathbf{g}\mathbf{g}'}) \frac{1}{(\varepsilon - \varepsilon_{\mathbf{k}+\mathbf{g}} + \mathrm{i}s)} + \ldots \tag{95}$$

In (95) $P_l(\theta)$ is the lth Legendre polynomial and $\theta_{gg'}$ is the angle between $k + g$ and $k + g'$.

Now suppose only one conduction band lies in the vicinity of ε_{f}, i.e. only $g = 0$ is important. Then (95) becomes

$$\frac{\mathrm{Tr}\,(G_{\mathrm{f}} - G_{\mathrm{f}}^0)}{N_s} = \sum_{\mathbf{K}} \frac{V^2 N}{(\varepsilon - \varepsilon_{\mathrm{f}})^2 (\varepsilon - \varepsilon_{\mathbf{K}} + \mathrm{i}s)} + \sum_{\mathbf{K}} \frac{V^4 N^2 N_s}{(\varepsilon - \varepsilon_{\mathrm{f}})^3 (\varepsilon - \varepsilon_{\mathbf{K}} + \mathrm{i}s)^2} + \ldots \tag{96}$$

where **K** is a vector anywhere in k-space. Recalling that V^2 is of $O(1/N)$, we see that the terms in (96) are both *of the same order*. Although the leading term constitutes the large-N limit of the impurity result, the second term is *not* down by $1/N$ and we do *not* retrieve the impurity result as the large-N limit.

In order to retrieve the impurity result as the large-N limit of the free-electron Anderson-lattice model, it seems that we have to scale the lattice parameter with N, a scaling with $N^{1/3}$ being a simple choice. Now there are many bands interacting with the f-levels, as in (95). The second term in (95) contains an extra factor N_s/v, and this now scales as N^{-1}. In fact each term of order V^{2r} in the expansion (95) formally contains N^{1-r} and the first term is left as the large-N limit, as desired.

As a check on whether the formal classification in powers of $1/N$ holds numerically we performed some calculations of the terms in the series (95), on a simple cubic lattice whose parameter scaled as $(2l + 1)^{1/3}$, for various energies ε. The results, illustrated in figure 17 as a function of energy, do bear out the trend for the ratio of the second to the first term in (95), though there is quite a lot of oscillation. Attempts to extend our calculation to higher orders encountered divergences which we have so far been unable to deal with.

The physics underlying this scaling of lattice parameter with N is that the number of conduction bands near ε_f should increase as N increases (as it does in the SU(N) lattice) otherwise we do not get enough bands to hybridize with the f-states. The

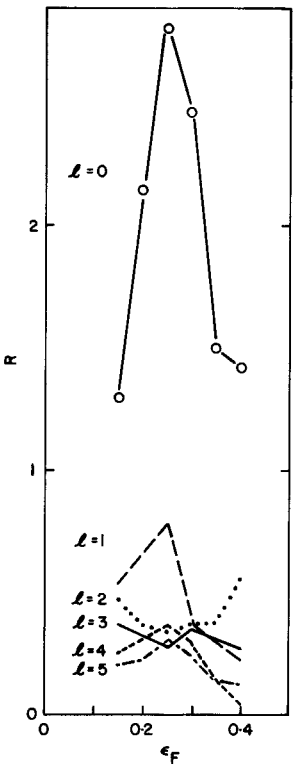

Figure 17. Ratio R of imaginary part of the second term of (95) to imaginary part of the first term, both evaluated at ε_F, plotted against ε_F, for various angular momenta l. The decrease in R with increasing l demonstrates the approach to the impurity model as the large-l limit.

choice of lattice parameter scaling with N ensures that the number of conduction electrons (and thus number of occupied conduction electron *states*) scales with f-electron degeneracy. We would argue that in practice metallic IV and heavy-fermion systems indeed do have a number of conduction electrons of order of or exceeding N (e.g. $CeSn_3$, $CeAl_3$, YbCuAl have 15, 12 and 7 valence electrons), justifying this approach.

In order that in the large-N limit the self-consistency relations should approach the impurity ones, first of all $\langle n_f \rangle$ should tend to the impurity value. Given that the imaginary part of (95) is replaceable by its first term as $N \to \infty$, then the foregoing result is assured on integrating over energy ε up to ε_F. The other expectation value required, $\Sigma_m \langle f_m^\dagger C_m \rangle$, is also related to (5.6)

$$\sum_{\mathrm{Im}} \langle f_m^\dagger c_m \rangle \sim \frac{-\mathrm{Im}}{\pi} \int_{-D}^{\varepsilon_F} \mathrm{d}\varepsilon \ \mathrm{Tr}\,[(\varepsilon - \varepsilon_f)G_f - 1], \tag{97}$$

and so indeed the self-consistency relations reduce to the impurity ones in the large-N limit provided we accept that higher terms in (95) vanish relative to the first.

The susceptibility χ of the f-electrons may be written

$$\chi \propto \sum_{m,m'} \frac{\partial}{\partial \varepsilon_{m'}} \langle n_m \rangle, \tag{98}$$

where we have made $\varepsilon_f = \varepsilon_m$ m-dependent. Again the quantity $\langle n_m \rangle$ is expressed in terms of G_{fmm} which possesses an expansion similar to (95). Formally, with scaling of the lattice parameter as $N^{1/3}$, the expansion is dominated by the first term as $N \to \infty$ leading to an impurity-like susceptibility as $N \to \infty$. However, no numerical checks have been done in this case as to the validity of the formal result.

The RKKY interaction may also be estimated in this model. If we quantize along the axis between two sites i and j where the spins are located, we retrieve the diagrams of figure 6. The RKKY energy is given by

$$E_{\mathrm{int}}(m, m) = 2J^2(4\pi)^2 P \int_0^{k_f} \mathrm{d}k\, k^2 \int_0^\infty \mathrm{d}k' \frac{k'^2}{\varepsilon_k - \varepsilon_{k'}} g_m(kR) g_m(k'R), \tag{99a}$$

where

$$g_m(kR) = 2\pi \int_1^{-1} \mathrm{d}x \exp(\mathrm{i}kRx)\, |Y_l^m(x)|^2. \tag{99b}$$

One limit of (99) is the Siemann–Cooper one [73], appropriate when $k_F R \to \infty$ at fixed l (in fact $k_f R \gg l(l+1)$). However, this limit is not the appropriate one in our case where R is scaling like $l^{1/3}$. Assuming, on the contrary, that $l \to \infty$ at fixed R, m we obtain a different limit. Taking $m = 0$, which is expected to give the largest interaction, we obtain in the large-l limit

$$E_{\mathrm{int}}(0, 0) \sim \frac{32\pi^2 J_0^2}{N^2} \int_0^{k_F} \mathrm{d}k\, k^2 J_0(kR) \int_0^\infty \frac{\mathrm{d}k'\, k'^2 J_0(k'R)}{\varepsilon_k - \varepsilon_{k'}} \tag{100}$$

where $N = 2l + 1$ and $J_0(x)$ is the ordinary Bessel function of zeroeth order. Equation (100) shows that again the RKKY interaction is of order N^{-2}, and therefore that the Kondo-lattice phase is stable in the large-N limit as shown by Coleman [39] and Read *et al.* [42].

In this subsection, we have followed a different line of reasoning (employing k-space Green functions) to that in [42] which employed real-space Green functions.

The latter proofs seem to demonstrate the same results as in the foregoing but the convergence of the real-space summations was a doubtful point. Suspiciously, the $N^{1/3}$ scaling of lattice constraint did not seem necessary in the real-space derivations. It is seen to be much more difficult to give convincing proofs of the large-N limit in the free-electron Anderson-lattice model than in the SU(N) Anderson lattice, which is also much more tractable for other purposes, e.g. calculating $1/N$ corrections. In point of realism the free-electron Anderson lattice is also little better than the SU(N) lattice. Therefore we think the SU(N) lattice (sometimes referred to as the 'spherical cow' model) is the best paradigm for an analytically tractable IV lattice model.

6. Realistic lattice models

In the foregoing, we have considered two model lattices, the SU(N) and free-electron lattice models, which lend themselves to analytic calculations, e.g. retrieval of the impurity model as the large-N limit. The SU(N) lattice also readily enables the case of the insulating IV system to be derived. However, one needs to assure oneself that the real features of IV systems s-, p-, d- as well as f bands, and relatively complex structures, may be taken into account in our picture.

From a model-Hamiltonian point of view we may write a more general extension of (59) as

$$H = \sum_{\mathbf{k}p\sigma} \varepsilon_{\mathbf{k}p} n_{\mathbf{k}p\sigma} + E_0 \sum_{im} f_{im}^\dagger f_{im} + \sum_{\mathbf{k}p\sigma,im} [V(\mathbf{k}p\sigma, m) f_{im}^\dagger c_{\mathbf{k}p\sigma} b_i \exp(-i\mathbf{k}\cdot\mathbf{R}_i) + \text{h.c.}] + \sum_i \gamma_i (b_i^\dagger b_i + n_{fi} - 1). \quad (101)$$

In (101) we retain for simplicity a lattice with one RE per unit cell; $\mathbf{k}$ is the Bloch wave-vector, p host-band index, σ spin, and i denotes the RE site (or unit cell) location R_i. b_i is once more the boson on site i, the remaining notations being analogous to (59). The transfer matrix element $V(\mathbf{k}p\sigma, m)$ between band $|\mathbf{k}p\rangle$ of spin σ to the f-state of angular momentum m at site R_0 is now relatively complex.

In mean-field approximation (101) may be written

$$H = \sum_{\mathbf{k}} h_{\mathbf{k}} + (\varepsilon_f - E_0) \sum_i (z + n_{fi} - 1), \quad (102)$$

where, writing $f_{km} = N_s^{-1/2} \Sigma_i f_{im} \exp(i\mathbf{k}\cdot\mathbf{R}_i)$,

$$h_{\mathbf{k}} = \sum_{p,\sigma} \varepsilon_{\mathbf{k}p} n_{\mathbf{k}p\sigma} + \varepsilon_f \sum_m f_{\mathbf{k}m}^\dagger f_{\mathbf{k}m} + z^{1/2} N_s^{1/2} \sum_{p\sigma,m} [V(\mathbf{k}p\sigma, m) f_{\mathbf{k}m}^\dagger c_{\mathbf{k}p\sigma} + \text{h.c.}]. \quad (103)$$

Now in order to proceed, we would have to calculate the band structure of the Hamiltonian $h_{\mathbf{k}}$. This is not easy because no reliable procedure exists for calculation of the matrix elements $V(kp\sigma, m)$.

In fact, we chose to employ the established and computationally efficient linearized muffin-tin orbital (LMTO) procedure [74]. Our procedure is best explained if we start by neglecting relativistic effects. Assuming that there is one atom per unit cell, and neglecting spin orbit, the LMTO Hamiltonian is, per spin,

$$h^k = C_l \delta_{L'L} + \tfrac{1}{2}\sigma\varphi_{l'}(-)[S^k(1 - \gamma S^k)^{-1}]_{L'L}\varphi_l(-). \quad (104)$$

In (104), $L = (l, m)$, σ is the atomic-sphere radius, $S^k_{L'L}$ are the structure constants, C_l is an effective centre of the lth band, while $\sigma\varphi_l^2$ is a potential parameter of the lth band. S^k depends only on crystal structure.

Now in order to write the model Hamiltonian equivalent to (104) requires us to ignore spin–orbit interaction and take m as pure orbital z-angular momentum, so (103) modifies to

$$h_{k\sigma} = \sum_p \varepsilon_p n_{kp\sigma} + \varepsilon_f \sum_m f^\dagger_{km\sigma} f_{km\sigma} + z^{1/2} N_s^{1/2} \sum_{p,m} [V(kp, m) f^\dagger_{km\sigma} c_{kp\sigma} + \text{h.c.}]. \quad (105)$$

Now (103) are in different representations; (103) employs a local basis throughout, (105) employs a local basis for $l = 3$, and a band-index basis for $l = 0, 1, 2$. However, it is evident that $z^{1/2}$ and $\varphi_3(-)$ both control the f-to-host hopping amplitude, and that ε_f and C_3 control the f-level.

The procedure we use [43] is based on the argument that the s, p and d bands of the system can be adequately calculated using the local density function (LDF) approximation. In this approximation, (104) may be iterated to self-consistency in the parameters C_l, φ_l. This is done for $l = 0, 1, 2, 3$. Then, using the analogy between (104) and (105), we renormalize the quantities $\varphi_3(-)$ and C_3 (γ_3 is negligible).

In fact there are large spin–orbit correction terms to (104) whose effect is to shift up the $f_{7/2}$ band so it is empty. The operative analogy is really between $C_{5/2}$ and ε_f, and $\varphi_{5/2}(-)$ and $f^{1/2}$, in (103) but our empirical procedure is adequate since we are not interested in its effect on the empty 7/2 band, only on the 5/2 band.

Our calculation was done on $CeSn_3$. First a relativistic LDF calculation was performed [44], then $\varphi_3(-)$ and C_3 were altered to renormalised values $\tilde{\varphi}_3(-)$ and $\tilde{C}_3$. These two parameters were controlled so as first to approximately satisfy the condition

$$z = 1 - \langle n_f \rangle = [\tilde{\varphi}_F(-)/\varphi_3(-)]^2. \quad (106)$$

Secondly we require that the specific heat, given by

$$\gamma = (\pi^2/3) k_B^2 \varrho(\varepsilon_F), \quad (107)$$

be in agreement with the experimental value, from which we deduce that the density of states $\varrho(\varepsilon_F)$ should be $306\,\text{Ry}^{-1}$.

It proved unnecessary to modify C_3, within the errors of our procedure, a fortuitous result. The value of $z = [\tilde{\varphi}_3(-)/\varphi_3(-)]^2$ was 0·11, in fair agreement with $1 - \langle n_f \rangle = 0{\cdot}14$, considering that in the LMTO theory the definition of $\langle n_f \rangle$ might differ somewhat from that appropriate to (103).

A first effect of introducing the renormalization effect z is on the pressure. We find that the pressure changed from -344 kbar in LDF to -39 kbar, a value which reflects the greatly reduced attractive contribution of the f-electrons to the ground-state energy.

The effect on the effective masses at the Fermi level is seen in table 4. We see that the renormalized effective masses are mostly much heavier, but one becomes lighter.

Table 4. Comparison of LDF, rescaled and experimental band masses.

LDF calculated mass m^*/m	Rescaled mass m^*/m	Experimental mass m^*/m	Plane in Brillouin zone
4–12	0·5–0·6	0·45	ΓXM
0·3–1·7	3·2–12		ΓXM
0·2–1·2	1·0–4·4	4·6	ΓXM
0·3–1·2	6–12	9	ΓXM
0·3–1·1	2–6	4·2–4·4	XMR

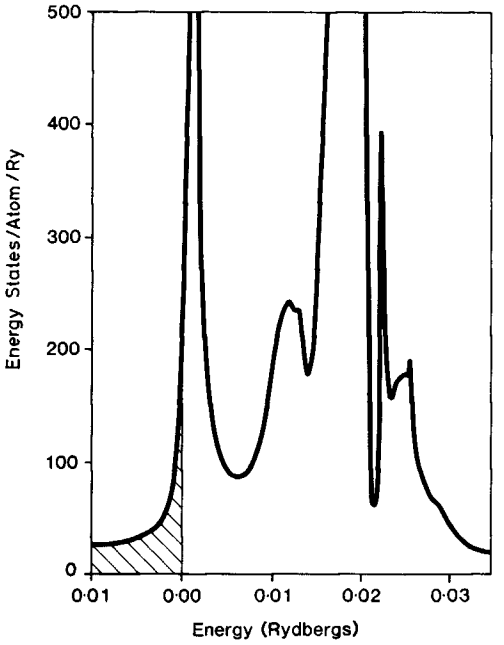

Figure 18. Density of states from the renormalized band structure of $CeSn_3$ [44], Fermi level as energy zero. The $j = 5/2$ DOS forms the single peak just above ε_F.

The renormalized masses are in much better agreement with experiment than are the LDF ones, including the predicted lighter mass for the small area Γ orbit which is indeed observed. The density of states in the renormalized band structure is illustrated in figure 18. We find that there is a narrow 5/2 peak $\sim 10\,\text{meV}$ above ε_f, and an unoccupied 7/2 peak much higher up. Qualitatively this resembles the Lorentzian density of states found for one impurity and which is the large-N limit of the foregoing lattice models. But quantitatively, the agreement with a Lorentzian is poor; a Lorentzian density of states satisfying $\langle n_f \rangle = 0{\cdot}89$, $\varrho(\varepsilon_f) = 308\,\text{Ry}^{-1}$, requires $\varepsilon_f = 34\,\text{meV}$. But, the peak in the DOS in figure 18 is at only 10 meV above ε_f.

We see that the renormalized band-structure calculation gives a reasonable picture of the pressure, effective masses, f-occupation and density of states in $CeSn_3$, while the LDF procedure does not. The density of states near ε_F is qualitatively, but not quantitatively, described by a Lorentzian resonance in the 5/2 channel.

7. The $U = \infty$ Hubbard model

Up to now we have considered the $U = \infty$ Anderson model and its extensions to the lattice. Another simpler model which has been used in the development of the theory of heavy-fermion systems is the Hubbard model. One regime where this model has recently been applied is to the lattice model of normal liquid He^3 [75]. In this application the model is specified to have one fermion per site and $N = 2$ (half-filled case), in which case Brinkman and Rice considered the mass enhancement as U approaches a critical value U_c (at which the metal–insulator transition occurs) from below. However, in heavy-fermion systems another regime, where U is very large and the occupation differs from half-filling, would be more appropriate [68].

We are then led to consider a Hubbard model with $U = \infty$. Within the large-N philosophy we shall assume it is N-fold degenerate, and also assume SU(N) symmetry. The model then takes the form

$$H = t \sum_{\langle ij \rangle m} f_{im}^{\dagger} f_{jm} b_j^{\dagger} b_i, \tag{108}$$

where we have assumed that only nearest neighbours i, j, denoted $\langle ij \rangle$, are coupled by the hopping-matrix element t. The constraint on (108) is

$$Q_i = \sum_m f_{im}^{\dagger} f_{im} + b_i^{\dagger} b_i = 1, \tag{109}$$

on each site i.

In mean-field theory, (109) is implemented only on average by adding the Lagrange multiplier term $\varepsilon_f(Q_i - 1)$ to H, and b, and $b_i^{\dagger}$ are replaced by $z^{1/2}$, to give

$$H_{mf} = zt \sum_{\langle ij \rangle m} f_{im}^{\dagger} f_{jm} + \varepsilon_f \sum_i (n_{fi} + z - 1) \tag{110}$$

(110) represents a non-interacting Hubbard model with renormalized hopping parameter zt, and f-energy level shifted from zero to ε_f. Varying ε_f and z leads to the self-consistency equations

$$n_f = -\frac{N}{\pi} \operatorname{Im} \sum_{\mathbf{k}} \int^{\mu} d\varepsilon \frac{1}{\varepsilon - \varepsilon_{\mathbf{k}} + is} = 1 - z \tag{111}$$

and

$$t \sum_{j,m} \langle f_{im}^{\dagger} f_{jm} \rangle = -t \frac{N}{\pi} \operatorname{Im} \sum_{\mathbf{k},j} \int^{\mu} d\varepsilon \frac{\exp [i\mathbf{k} \cdot (\mathbf{R}_j - \mathbf{R}_i)]}{\varepsilon - \varepsilon_{\mathbf{k}} + is} = -\varepsilon_f. \tag{112}$$

In (112) the j-sum is only over the nearest neighbours to i. Defining

$$\varrho(\varepsilon) = -\frac{1}{\pi} \operatorname{Im} \sum_{\mathbf{k}} \frac{1}{\varepsilon - \varepsilon_{\mathbf{k}} + is}, \tag{113}$$

(111) may be written

$$N \int^{\mu} d\varepsilon \, \varrho(\varepsilon) = 1 - z. \tag{114}$$

By means of a well known trick, involving the fact that j is the nearest neighbour of i, i.e.

$$\varepsilon_{\mathbf{k}} = \varepsilon_f + zt \sum_i \exp [i\mathbf{k} \cdot (\mathbf{R}_j - \mathbf{R}_i)], \tag{115}$$

(112) may be rewritten in the form

$$\frac{N}{z} \int^{\mu} d\varepsilon \, (\varepsilon - \varepsilon_f) \varrho(\varepsilon) = -\varepsilon_f, \tag{116}$$

involving the first moment of $\varrho(\varepsilon)$.

Thus (114) and (116) show that the self-consistency relation only involves the density of states. Taking then a simple model form for the bare density of states

$$\varrho_0(\varepsilon) \begin{cases} = 1/2D, & -D < \varepsilon < D, \\ = 0, & |\varepsilon| > D, \end{cases} \tag{117}$$

we have

$$\varrho(\varepsilon)\begin{cases} = 1/2zD, & -zD < \varepsilon < zD, \\ = 0, & |\varepsilon| > zD, \end{cases} \tag{118}$$

and (114) and (116) become

$$n_f = (N/2zD)(\mu - \varepsilon_f + zD) = 1 - z, \tag{119}$$

$$(N/2zD)[\tfrac{1}{2}(\varepsilon_f - \mu)^2 - \tfrac{1}{2}(zD)^2] = -\varepsilon_f z. \tag{120}$$

The self-consistent relation (120) here, in contrast to the Anderson case does not contain a logarithm; hence there is no exponentially small Kondo temperature found in the Hubbard model. This is perhaps a point against the Hubbard and in favour of Anderson-lattice models of heavy-fermion materials, since the materials are precisely those where the characteristic temperature is very low. From (119) and (120)

$$\varepsilon_f = Dn_f[1 - (n_f/N)]. \tag{121}$$

As usual, χ and γ are Fermi-liquid properties given by the DOS at μ;

$$\chi_0 = \tfrac{1}{3}j(j+1)(g\mu_B)^2 \frac{N}{2D(1-n_f)}, \tag{122a}$$

$$\gamma = \frac{\pi^2}{3} k_B^2 \frac{N}{2D(1-n_f)}. \tag{122b}$$

These quantities become very large as $n_f \to 1$, qualitatively as in the Anderson-lattice models.

It is straightforward to solve (119) and (120) for μ and obtain the charge susceptibility

$$\chi_c = \frac{1}{n_f^2}\frac{dn_f}{d\mu} = \frac{1}{2Dn_f^2\left(1 + \frac{1}{N} - \frac{3n_f}{N}\right)}. \tag{123}$$

The ground-state energy of the model is

$$E_0 = N\int^{\mu} d\varepsilon\, \varepsilon\varrho_f(\varepsilon) + \varepsilon_f(z-1), \tag{124}$$

$$= -(1-n_f)n_f[1 - (n_f/N)]D. \tag{124}$$

We see that the SU(N) Hubbard model in mean field has some points in common with the SU(N) Anderson lattice, e.g. χ and γ diverge as $n_f \to 1$, but no exponentially small Kondo temperature appears. The band narrows by the factor $(1 - n_f)$ and shifts upwards until it is close to the original upper band edge. However, the charge susceptibility, although it is small (of order $1/2D$ for large N, $n_f \to 1$), does not vanish as $n_f \to 1$ as it does in the Anderson models.

The Brinkman–Rice theory [75], in the large-U limit, also has a similar mass-enhancement, equivalent to $z = 2(1 - n_f)$ as $n_f \to 1$. Our mean-field theory is thus in agreement with the Brinkman–Rice variationally derived theory, except for the extra factor discussed in §4.6, which is essentially a $1/N$ correction. The mean-field approach has the advantage of simplicity and straightforward extension to finite (low) temperatures.

In one dimension, the $N = 2$ Hubbard model is exactly soluble for any U and any n_f. It is found that in the $U \to \infty$ limit at fixed $n_f < 1$ the susceptibility diverges,

contrary to (122*a*). We believe this is a peculiar result of the low dimensionality, arising from the fact that in one dimension the impenetrable particles cannot cross one another, and behave like spins. This physical argument is also applicable to any N, and if correct suggests that χ should also diverge as $U \to \infty$ for any n_f at $N > 2$. Then (122*a*) could not be correct in one dimension. At higher dimensionalities the particles can get round each other and the problem disappears. The argument in this paragraph seems then to introduce some doubt as to whether mean field is the true large-N limit of this model, but it is only intuitive since we do not have the exact solution to Hubbard for $N > 2$.

8. Tm impurity

The Tm ion differs from the Ce, Yb, Sm and Eu ions (at least in their ground states) in that its two valence states, f^{12} and f^{13}, are both magnetic, with degeneracies 13 and 8, respectively. Indeed TmSe is completely different in its properties from other IV materials, presumably due to this feature of the RE ion [76]. Even greater interest in the case of ions with two magnetic valences comes from the U ion, which is probably fluctuating between the f^2 and f^3 states [77]. The U ion is of great importance in forming heavy-fermion materials such as UBe_{13} which are also superconducting, probably as non-s-wave single superconductors and therefore of great fundamental interest.

Previous treatments have considered the Tm ion within a variational framework, without use of the large-N expansion [47]. In order to establish results with less ambiguity, Read *et al.* [48], using however the Keiter–Kimball formalism, repeated this calculation in a large-N framework; they obtained energy scales analytically for the first time and checked them against Haldane-scaling results. They were able to establish the validity of the leading-N calculation in which limit the calculation of [47] is correct. Nunes, Rasul and Gehring (preprint) extended this approach to the U ion, using however an extension of the variational technique [37] to treat the f^0–f^1–f^2 problem. In the following we rederive the results of [48] by the slave-boson approach, introducing a modified mean-field technique. This allows the procedures of [48] to be extended to the lattice.

In this section we shall consider an f^1–f^2 ion (the equivalent to f^{12}–f^{13}) in the somewhat artifical model which has SU(N) symmetry used by Read *et al.* [48]. This means that f^1 has degeneracy N, f^2 has degeneracy $N(N-1)/2$. If $N = 8$, the f^2 degeneracy of the model is 28, in contrast to 13 for Tm^{3+}. The degeneracy of the f^2 is thus exaggerated by the SU(N) model. It is important for large-N theory that the ratio of the f^2 to f^1 degeneracy be itself proportional to N, as it is in the SU(N) model.

The model of the f^1–f^2 SU(N) impurity is then, in bosonized form,

$$H = \sum_{k,m} \varepsilon_k c^\dagger_{km} c_{km} + E_f \sum_m f^\dagger_m f_m + V \sum_{k,m \neq n} (b_{mn} f^\dagger_m c^\dagger_{kn} + \text{h.c.}), \tag{125}$$

with a constraint

$$Q = \sum_{m>n} b^\dagger_{mn} b_{mn} + \sum_m f^\dagger_m f_m = 1. \tag{126}$$

Now we have in (125) a tensor boson $b_{mn} \equiv -b_{nm}$, $n \neq m$, with $N(N-1)/2$ independent components, which describes the f^2 state, while the fermion f_m describes the f^1 state. The energy E_f is defined as $E_f = E_1 - E_2$, where E_1 is the total energy of the f^1 state, E_2 of the f^2 state, (ε_F taken as energy zero).

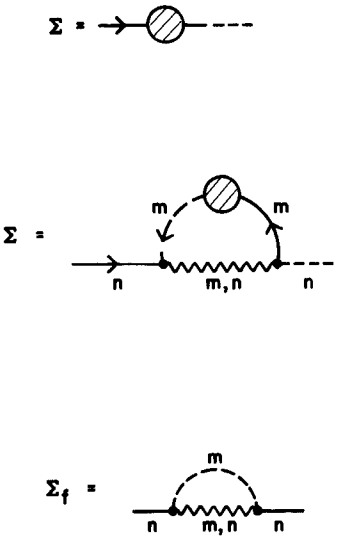

Figure 19. (*a*) The f-conduction band self-energy $\Sigma(\omega)$ introduced into the model for a Tm impurity in leading order in $1/N$. Full line, f-propagator, broken line, k-propagator. (*b*) Expression for $\Sigma(\omega)$ in terms of itself. Filled circles indicate V-vertex in (125), wavy line is tensor boson. (*c*) Self-energy correction to f-line in leading order.

The mean-field theory of (125) and (126) is presented here for the first time. First we introduce the Lagrange multiplier procedure as before, to get the Hamiltonian

$$H' = \sum_{k,m} \varepsilon_k c^\dagger_{km} c_{km} + \varepsilon_f \sum_m f^\dagger_m f_m + V \sum_{kmn} (b_{mn} f^\dagger_m c^\dagger_{kn} + \text{h.c.}) + \gamma \left[\sum_{m>n} b^\dagger_{mn} b_{mn} - 1 \right], \tag{127}$$

with $\gamma = (\varepsilon_f - E_f)$ as the Lagrange multiplier. The meaning of (127) seems to be that ε_f is the energy difference $(E_1 - \varepsilon_0)$, and γ is the difference $(E_2 - \varepsilon_0)$, where ε_0 is the energy of the ground-state singlet, in the notation of [48].

Now we cannot just take the expectation value $\langle b_{nm} \rangle$, as before, because the boson being a tensor would break SU(N) symmetry. However (127) is a conventional Hamiltonian for which we can use Feynman diagrams. We introduce a self-energy $\Sigma(\omega)$ which has the gauge symmetry-breaking property of the $\langle b \rangle$ expectation value in f^1–f^0 theory, i.e. it has an f-line entering and a k-line leaving (figure 19 (*a*)). Then we write a self-consistent equation for Σ in terms of itself (figure 19 (*b*)). In figure 19 (*b*) the wavy line represents the tensor boson. Because of the internal summation over m, figure 19 (*b*) represents the leading-N diagram.

In order to evaluate figure 19 (*b*), we introduce conventional Feynman $T = 0$ diagrams for the fermion propagators, G^0_f and G^0_k. The propagator for the boson is

$$\begin{aligned} D(t) &= -i\langle T b^\dagger(0) b(t) \rangle, \\ D(\omega) &= 1/(\omega - \gamma + is). \end{aligned} \tag{128}$$

The fermion propagators are

$$\begin{aligned} G^0_f(\omega) &= 1/(\omega - \varepsilon_f + is) \\ \sum_k G^0_k(\omega) &= \sum_k \frac{1}{\omega - \varepsilon_k + is \operatorname{sgn} \varepsilon_k} \simeq -i\pi \operatorname{sgn} \varepsilon_k . \end{aligned} \tag{129}$$

First working with an unrenormalized f-propagator, the diagram of figure 19(*b*) yields the expression

$$\Sigma(\omega) = \frac{(N-1)V^2}{2\pi i}\int_c d\omega'\, D(\omega+\omega')G_f(\omega')\Sigma(\omega')\sum_k G_k^0(\omega'), \tag{130}$$

where C is a contour along the real axis completed in the upper half plane. Introducing

$$Z(\omega) = \Sigma(\omega)G_f^0(\omega)\sum_k G_k^0(\omega), \tag{131}$$

(130) becomes

$$(\omega-\varepsilon_f)Z(\omega) = \frac{(N-1)V^2}{2\pi i}\sum_k G_k^0(\omega)\int_c d\omega' \frac{Z(\omega')}{\omega+\omega'-\gamma+is}. \tag{132}$$

Distorting the contour in (132) to encircle the cut in $Z(\omega)$, which may be introduced as

$$Z = X + iY$$

valid on the real axis, we have

$$(\omega-\varepsilon_f)Z(\omega) = \frac{(N-1)V^2}{\pi}\sum_k G_k^0(\omega)\int_{-\infty}^0 \frac{Y(\omega')\,d\omega'}{\omega+\omega'-z}. \tag{133}$$

In fact, the integral in (133) is non-singular. Taking the imaginary part of (133) we have

$$(\omega-\varepsilon_f)Y(\omega) = \Gamma\int_{-\infty}^0 \frac{Y(\omega')\,d\omega'}{\omega+\omega'+E_f-\varepsilon_f}, \tag{134}$$

where $\Gamma = V^2(N-1)\varrho$.

Finally, we introduce the leading-N self-energy, figure 19(*c*), of the f-propagator. This results in a correction in the $(\omega-\varepsilon_f)$ factor in (134), which becomes

$$\omega-\varepsilon_f \to \omega-\varepsilon_f-\Gamma\int_{-D}^0 d\varepsilon' \frac{1}{\varepsilon'+\omega+E_f-\varepsilon_f}. \tag{135}$$

Inserting this into (134), we may write the result

$$Y(\omega)(\omega-\varepsilon_f) = \Gamma\int_{-\infty}^0 \frac{[Y(\omega')+Y(\omega)]\,d\omega'}{\omega+\omega'+E_f-\varepsilon_f}. \tag{136}$$

This is a homogeneous equation from which ε_f may be determined in terms of the known quantity $E_f = E_1 - E_2$. It is identical to equation (3.15) of [48].

In [48] we have solved the integral equation by several methods. There are two Kondo limits, $n_f = 1$ and $n_f = 2$, so the energy scale vanishes at both the limits. Actually, results even in the Kondo limit depend on whether D or $|E_f|$ goes to infinity first; the former case is considered here. The energy scale $\tilde{\varepsilon}_f$ is defined with respect to an f^1 state itself renormalized by the self-energy of figure 19(*c*). We introduce a characteristic scale T^* by

$$T^* = -E_f + \Gamma\ln(D/T^*). \tag{137}$$

Then

$$\tilde{\varepsilon}_f = \varepsilon_f - \Gamma\ln(D/T^*). \tag{138}$$

In the f^2 Kondo limit

$$\tilde{\varepsilon}_f = D\exp(-E\Gamma), \tag{139}$$

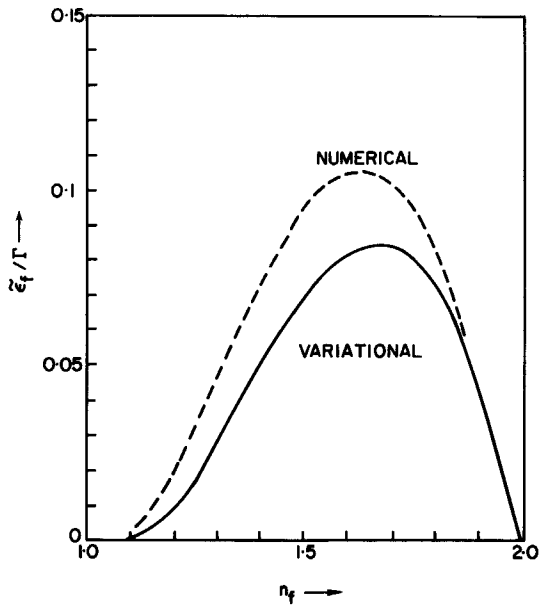

Figure 20. Energy lowering $\tilde{\varepsilon}_f$ of singlet ground state of Tm impurity model below N-multiplet, as a function of n_f. Note that the Kondo limit of $n_f \to 1$ differs from that of $n_f \to 2$. Full line, variational solution to (136), broken line numerical solution.

while in the f^1 Kondo limit

$$\tilde{\varepsilon}_f = (T^{*2}/D) \exp(E\Gamma), \tag{140}$$

where $\Gamma = (N-1)V^2\varrho$.

A numerical solution of the integral equation in the $D \to \infty$ limit is illustrated in figure 20. It shows that the two Kondo limits are asymmetrical, as indicated by the different formulae (139) and (140).

In this section we have, we believe for the first time, given correctly the mean-field approach to the f^1–f^2 (Tm-like) impurity. In this way the Varma–Yafet [47] integral equation (136), known to be correct in the large-N limit, has been rederived.

The mean-field derivation is more canonical than the one previously used. It provides a natural explanation of why the function $Y(\omega)$ was found in [48] (where it is termed $B(\omega)$) to be peaked at small $-\omega$; this is becase of the factor $G_f(\omega)$ defined into it. Most importantly, the mean-field approach is straightforwardly extensible to the lattice. It is then found that, as for the f^0–f^1 SU(N) lattice, we get back a band structure having $N = 8$-fold degeneracy and the same energy scale as for the single impurity (Newns, unpublished work).

Unfortunately, the large-N theory of the SU(N) f^1–f^2 model seems to lead qualitatively to very similar physics to that of the f^0–f^1 model. We do not arrive at a simple explanation [48] of the magnetism of TmSe, and of the very low or zero Kondo temperature of Tm impurities [48], based on the magnetism of both of the Tm valence states, as had been expected [76].

9. Beyond mean field

In this section we wish to diverge slightly from the central theme of this article and indicate briefly the nature of some of the effects found by going beyond the mean-field approximation.

First of all, there is no true symmetry breaking. This is a consequence of the local gauge symmetry of the model, i.e. the fact that Q_i commutes with H, where Q_i in (59) is the generator of a rotation in phase of b_i and f_i, for example

$$\exp(-i\phi Q_i)\, b_i \exp(i\phi Q_i) = b_i \exp(i\phi)$$

for an arbitrary phase angle ϕ. Only physical quantities, such as $f_{im}^\dagger f_{im}$, transforming like unity under the gauge transformation, may have non-zero expectation values. Consequently the boson autocorrelation function does not approach a constant at large times, but falls off as the inverse $(1/N)$th power of the time, indicating that symmetry is nearly, but not quite, broken [40].

Next, while mean-field theory gives a picture of non-interacting quasiparticles, in reality there is quasiparticle–quasiparticle interaction leading first of all to thermodynamic effects such as deviations in the χ/γ ratio from unity. Possible approaches to calculating such effects are via exact solutions, Fermi-liquid theory or calculating terms of order $(1/N)$ in the slave boson or other $1/N$ approaches. A good approximation to the χ/γ ratio for the infinite-U SU(N) impurity is obtained by calculating the $1/N$ corrections to mean field (figure 7(*b*)) as [43]

$$\pi^2 k_B^2 \chi/\mu_{\text{eff}}^2 \gamma = N/[N - 1 + (n_f - 1)^2]. \tag{141}$$

This agrees up to leading and next-leading order in $1/N$ with the exact linear relation between χ, γ and χ_C found by Fermi-liquid theory [49], and with the numerical work of Zhang and Lee [35]. Equation (141) shows that χ/γ is 1 for small n_f (the infinite U has little effect here) and $1 + 1/(N - 1)$ for $n_f \to 1$, the exact result for a Kondo impurity [24–28, 49].

For the lattice, the Fermi-liquid theory of the SU(N) model seems not yet to have been considered correctly, but for the spin-$\frac{1}{2}$ lattice Fermi-liquid theory [72] is unable to determine χ/γ even in the Kondo limit. It only gives constraints on various quantities. By carrying out the fluctuation corrections to mean field, $\chi(0)$ and $C_V(T)$ have been calculated recently [44, 45]. The χ/γ ratio is claimed to be $1 + N^{-1} + O(N^{-2})$ in the Kondo limit [44, 45]. An interesting result is the presence of a $T^3 \ln T$ term in the specific heat, though this is now believed to be small (A. J. Millis, preprint).

In mean field, the density of states for the single impurity problem is the Lorentzian of figure 6. However, this is the quasiparticle density of states. If we wish to calculate the density of states of 'real electrons', we have to start from the Green function $G_f^e(t) = -i\langle T f_m(t) b^\dagger(t) f_m^\dagger(0) b(0)\rangle$. In mean field, this is just z times the quasiparticle Green function G_f so that z is the renormalization factor by which the quasiparticle DOS is to be multiplied to get the 'real electron' DOS [40, 42]. However, if we calculate G_f^e beyond mean field (say to $O(1/N)$) it amounts to convolution of G_f with the bubble-sum (RPA) boson propagator [41]. This introduces an asymmetry into the quasiparticle peak, due to the infrared singularity of the conduction electrons, and adds a satellite approximately at E_f plus the excitation energy of the boson, i.e. at $\varepsilon_f + (E_0 - \varepsilon_f) = E_0$ [37, 42]. This satellite is clearly seen in the ultraviolet photoemission (UPS) spectra of Ce IV systems [6]. It is very broad, of width $N\Delta_0$ [37, 42]. The theory and comparison with experiment for UPS and other spectroscopies have been studied in great detail by Gunnarsson and Schonhammer [37, 41].

For impurities a very interesting transport property is the thermopower $S(T)$ [10]. Recently an identity for the T-linear coefficient of S has been established by Kawakami, Usuki and Okiji (preprint), valid for the SU(N) Anderson model

$$S(T) = 2(\pi/eN)\gamma T \cot(\pi n_f/N). \tag{142}$$

Table 5. Thermopowers. The values calculated from equation (42) are compared to experimental values.

	γ (mJ K^{-2})	Experiment S/T (μV K^{-2})	Theory S/T (μV K^{-2})
YbCuAl	260	−4·0	−5·1
$YbCu_2Si_2$	135	−1·0	−2·65
$YbAl_3$	45	−0·6	−0·88
$CeSn_3$	53	0·13	0·99
$CePd_3$	37	1·5	0·70

Equation (142) shows that S/T should be positive for Ce compounds, negative for Yb compounds (where $N = 8$, $n_f = 7$–8) and should scale with gamma. In fact, since the effect of going beyond mean field is only a factor $(1 - 1/N)$ in γ the mean-field approximation to (142), would be adequate. In table 5 we test (142) in actual IV materials [10]. The results are good for the Yb materials, except for $YbCu_2Si_2$ wherethe discrepancy is probably due to crystal-field effects, but quantitatively poor for the Ce materials. This may be essentially a test of how good a local or impurity-like approximation is.

As has long been known, in the dilute limit the resistivity at zero temperature of an ensemble of SU(N) impurities of concentration n_i is (n = concentration of electrons):

$$\varrho = \frac{2\pi n_i}{ne^2 k_F} N \sin^2\left(\frac{\pi n_f}{N}\right). \tag{143}$$

Essentially the $T = 0$ resistivity is related [27] only to the cross-section and thus to the sine squared of the phase shift, which is itself related to n_f by the sum rule. The temperature dependence of ϱ has been discussed by Houghton *et al.* [78]. Similarly a simple result exists for the zero-temperature magnetoresistance [24].

The resistivity of the perfect lattice, however, vanishes if there is no quasiparticle–quasiparticle interaction and is thus zero in mean field. It is also zero even in the presence of quasiparticle–quasiparticle interactions, in the absence of the periodic lattice. Studies using the $1/N$ approach show that ϱ scales with $(T/T_K)^2$ at low temperatures, [41] in agreement with experimental data [79].

10. Conclusion

In all the models considered in this paper mean-field approximation involves breaking the local gauge symmetry on lattice site i by introducing an expectation value $\langle b_i \rangle$ of the non-gauge-symmetric boson b_i on site i. Strictly speaking $\langle b_i \rangle$ is zero. In fact there is a power-law decay of the boson autocorrelation function in time which seems to ensure that breaking symmetry in this way at low temperatures is non-catastrophic but can be corrected by adding well behaved corrections of order $1/N$.

The mean-field approximation, and also the approximation of satisfying the constraint $Q = 1$ in only an average way, are valid only at very low temperatures $T < T_K$. In this regime, we see that mean field can be extremely accurate (figure 10) provided the number of channels N is reasonably large.

Mean field applied to the single impurity leads to a simple N-channel Lorentzian quasiparticle resonance near the Fermi level. The width of the resonance is renormalized

(in the Ce case) by the $z = 1 - n_f$ factor from its value in the absence of electron–electron interaction. The resonance adjusts its position so as to contain the correct number of f-electrons, i.e. it is above ε_F for Ce ($N = 6$, $n_f \leqslant 1$), and below ε_F for Yb ($N = 8$, $n_f \geqslant 7$). Specific-heat coefficient γ and magnetic susceptibility χ are simply related to the density of states at ε_F, which can be very high if $n_f \to 1$. The thermopower in mean field is related to the energy derivative of the DOS at ε_F, and is positive for Ce and negative for Yb materials. Similarly, quantities such as $d^2\chi(T)/dT^2$ and $d^3C_V(T)/dT^3$ at $T = 0$, and $d^3M(h)/dh^3$ at $h = 0$ are nearly related to the second derivative of the density of states at ε_F, and are positive. All the above properties of impurity systems scale inversely with the characteristic energy scale T_K, which may be very small.

For the lattice, mean field leads to a picture of non-interacting quasiparticles in bands whose mass is increased by the renormalization factor $z^{-1} = (1 - n_f)^{-1}$. Once again the high specific heats and susceptibilities are related to the inverse temperature scale T_K^{-1}. In the case of insulating IV systems, a simple explanation is provided in terms of a filled quasiparticle band separated by an absolute gap (which is narrowed by $\sim z$) from an empty band. In the limit of large N, the metallic IV systems are shown (most convincingly in the SU(N) model), to have impurity-like thermodynamic properties.

Based on the result just mentioned we can make contact between the theoretical results for the lattice and experimental observations on IV systems, which closely resemble the SU(N) impurity as regards their thermodynamic properties.

Improvement of mean field takes the form of calculating additional terms in the $1/N$ expansion. If this is done to order $1/N$ (involving RPA-like diagrams for the boson field), we can obtain such physical quantities as the f^0 satellite in the UPS spectrum and non-zero resistivity of the Anderson lattice. In addition, smaller effects such as deviations from unity in the χ/γ ratio can be obtained.

In the case of the thulium ion, which has both valences magnetic, a tensor rather than scalar boson has to be introduced. A different kind of formulation of mean field is needed to avoid breaking SU(N) symmetry.

Finally, we see that heavy-fermion superconductivity is a low-temperature problem ($T \ll T_K$), and large-N procedures, starting out from mean field, seem a very useful starting point for approaching it.

Acknowledgment

N. Read is grateful to the Science and Engineering Research Council of the U.K. for financial support.

References

[1] VARMA, C. M., 1976, *Rev. mod. Phys.*, **48**, 219.
[2] HEWSON, A. C., 1979, *J. Magn. magn. Mater.*, **12**, 83.
[3] LAWRENCE, J. M., RISEBOROUGH, P. M., and PARKS, R. D., 1981, *Rep. Prog. Phys.*, **44**, 1.
[4] STEWART, G. R., 1984, *Rev. mod. Phys.*, **56**, 755.
[5] LEE, P. A., RICE, T. M., SERENE, J. W., and WILKINS, J. W., 1986, *Comments in Condensed Matter Physics*, **12**, 99.
[6] LANG, J. K., BAER, Y., and COX, P. A., 1981, *J. Phys.* F, **11**, 3; BAYER, Y., and SCHOENES, J., 1980, *Solid St. Commun.*, **33**, 885; BAER, Y., OH, H. R., and ANDRES, R., 1980, *Solid St. Commun.*, **36**, 387.
[7] HERBST, J. F., WATSON, R. E., and WILKINS, J. W., 1976, *Phys. Rev.* B, **13**, 1439.

[8] COQBLIN, B., 1977, *The Electronic Structure of Rare Earth Metals and Alloys: The Magnetic Heavy Rare Earths* (New York: London: Academic Press).
[9] WILSON, K. G., 1975, *Rev. mod. Phys.*, **47**, 773.
[10] JAQUARD, D., and SIERRO, J., 1982, *Valence Instabilities*, edited by P. Wachter and H. Boppart (Amsterdam: North-Holland), p. 409.
[11] NEWNS, D. M., and HEWSON, A. C., 1980, *J. Phys.* F, **10**, 2428.
[12] PENNEY, T., MILLIKAN, F. P., VON MOLNAR, S., HOLTZBERG, F., and FISK, Z., 1987, *Phys. Rev. Lett.* (to be published).
[13] LEGGETT, A. J., 1975, *Rev. mod. Phys.*, **47**, 331.
[14] HIRST, L. L., 1974, *J. Phys. Chem. Solids*, **35**, 1285.
[15] ANDERSON, P. W., 1961, *Phys. Rev.*, **124**, 41.
[16] COQBLIN, B., and SCHRIEFFER, J. R., 1969, *Phys. Rev.*, **185**, 847.
[17] BRINGER, A., and LUSTFELD, H., 1977, *Z. Phys.* B, **28**, 213; LUSTFELD, H., and BRINGER, A., 1978, *Solid St. Commun.*, **28**, 119.
[18] NEWNS, D. M., and HEWSON, A. C., 1980, *J. Phys.* F, **10**, 2429.
[19] KLAASE, J. C. P., DE BOER, F. R., and DE CHATEL, P. F., 1981, *Physica* B, **106**, 178.
[20] MATTENS, W. C. M., 1980, Ph.D. Thesis, University of Amsterdam; MATTENS, W. C. M., ELLENBAAS, R. A., and DE BOER, F. R., *Commun. Phys.*, **2**, 147.
[21] POTT, R., SCHEFZYK, R., and WOHLLEBEN, D., 1981, *Z. Phys.* B, **44**, 17.
[22] RAJAN, V. J., 1983, *Phys. Rev. Lett.*, **51**, 308.
[23] HEWSON, A. C., RASUL, J. W., and NEWNS, D. M., 1983, *Solid St. Commun.*, **47**, 59; HEWSON, A. C., and RASUL, J. W., 1983, *J. Phys.* C, **16**, 3273.
[24] ANDREI, N., and LOWENSTEIN, J. H., 1981; *Phys. Rev. Lett.*, **46**, 356; ANDREI, N., and LOWENSTEIN, J. H., 1983, *Rev. mod. Phys.*, **55**, 331.
[25] HEWSON, A. C., and RASUL, J. W., 1982, *Phys. Lett.* A, **92**, 95.
[26] TSVELICK, A. M., and WIEGMANN, P. B., 1982, *J. Phys.* C, **15**, 1707; 1983, *J. Phys.* C, **16**, 2281, 2321.
[27] SCHLOTTMAN, P., 1983, *Phys. Rev. Lett.*, **50**, 1697; 1983, *Z. Phys.*, **51**, 3, 223.
[28] OKIJI, A., and KAWAKAMI, N., 1983, *Phys. Rev. Lett.*, **50**, 1157.
[29] HEWSON, A. C., NEWNS, D. M., RASUL, J. W., and READ, N., 1985, *J. Magn. magn. Mater.*, **47, 48**, 354.
[30] YOSHIMORI, A., and SAKURAI, A., 1970, *Prog. theor. Phys, Osaka Suppl.*, **46**, 162.
[31] LACROIX, C., and CYROT, M., 1979, *Phys. Rev.* B, **20**, 1969.
[32] KEITER, H., and KIMBALL, J. C., 1971, *Int. J. Magn.*, **1**, 233.
[33] MOVAGHAR, B., 1971, Thesis, University of London.
[34] RAMAKRISHNAN, T. V., and SUR, K., 1982, *Phys. Rev.* B, **26**, 1798.
[35] ZHANG, F. C., and LEE, T. K., 1983, *Phys. Rev.* B, **28**, 33.
[36] RASUL, J. W., and HEWSON, A. C., 1983, *J. Phys.* C, **16**, L933; 1984, **17**, 377.
[37] GUNNARSSON, O., and SCHONHAMMER, R., 1985, *Phys. Rev.* B, **31**, 4815; 1983, *Ibid.*, **28**, 4315.
[38] READ, N., and NEWNS, D. M., 1983, *J. Phys.* C, **16**, 3273.
[39] COLEMAN, P., 1983, *Phys. Rev.* B, **28**, 5255.
[40] READ, N., and NEWNS, D. M., 1983, *J. Phys. C*, **16**, L1055; NEWNS, D. M., READ, N., and HEWSON, A. C., 1984, *Moment Formation in Solids*, Proc. NATO Summer School, Vancouver Island W.L. Buyers (NATO ASI Series B, Vol. 117); READ, N., 1985, *J. Phys.* C, **18**, 2651; READ, N., 1986, Ph.D. Thesis, University of London.
[41] COLEMAN, P., 1984, *Phys. Rev.* B, **29**, 3035; 1987, *Phys. Rev.* B, **35**, 5072.
[42] READ, N., NEWNS, D. M., and DONIACH, S., 1984, *Phys. Rev.* B, **30**, 3841.
[43] READ, N., and NEWNS, D. M., 1984, *Solid St. Commun.*, **52**, 993; STRANGE, P., and NEWNS, D. M., 1986, *J. Phys.* F, **16**, 335; RAZAFIMANDIMBY, H., FULDE, P., and KELLER, J., 1984, *J. Phys.* B, **54**, 111.
[43] AUERBACH, A., and LEVIN, K., 1986, *Phys. Rev. Lett.*, **57**, 877; 1986, *Phys. Rev.* B, **34**, 3524; RASUL, J. W., and DESGRANGES, H.-U., 1986, *J. Phys.* C, **129**, L671.
[45] MILLIS, A. J., and LEE, P. A., 1987, *Phys. Rev.* B, **35**, 3394.
[46] MARTIN, R. M., 1982, *Phys. Rev. Lett.*, **48**, 362.
[47] YAFET, Y., VARMA, C. M., and JONES, B., 1985, *Phys. Rev.* B, **32**, 360.
[48] READ, N., DHARAMVIR, K., RASUL, J. W., and NEWNS, D. M., 1986, *J. Phys.* C, **19**, 1597.

[49] YOSHIMORI, A., 1976, *Prog. theor. Phys., Osaka*, **55**, 67.
[50] KOJIMA, H., KURAMOTO, Y., and TACHIKI, M., 1984, *Z. Phys.* B, **54**, 95; KURAMOTO, Y., and KOJIMA, H., 1984, *Z. Phys.* B, **57**, 142.
[51] BICKERS, N. E., COX, D. L., and WILKINS, J. W., 1985, *Phys. Rev. Lett.*, **54**, 230.
[52] HALDANE, F. D. M., 1978, *Phys. Rev. Lett.*, **40**, 416; 1978, *J. Phys.* C, **11**, 5015.
[53] KAWAKAMI, N., and OKIJI, A., 1985, *J. phys. Soc. Japan*, **54**, 685; OKIJI, A., and KAWAKAMI, N., 1985, *Proceedings of the International Conference on Magnetism*, San Fransisco 1985.
[54] DESGRANGES, H.-U., and RASUL, J. W., 1985, *Phys. Rev.* B, **32**, 6100; DESGRANGES, H.-U., 1985, *J. Phys.* C, **18**, 5481.
[55] JAYAPRAKASH, C., KRISHNAMURTHY, H. R., and WILKINS, J. W., 1981, *Phys. Rev. Lett.*, **47**, 737.
[56] LAVAGNA, M., and CYROT, M., 1985, *Solid St. Commun.*, **55**, 555.
[57] JONES, B. A., and VARMA, C. M., 1987, *J. Magn. magn. Mater.*, **63**, 64; 1987, *Phys. Rev. Lett.* (to be published).
[58] KOELLING, D. D., 1981, *Rep. Prog. Phys.*, **44**, 139; 1982, *Solid St. Commun.* **43**, 247; A. YANASE, 1982, *J. Magn. magn. Mater.*, **31–34**, 453.
[59] HARRIS, I. R., and RAYNER, G. V., 1965, *J. less-common Metals*, **9**, 7.
[60] MULLER-HARTMAN, E., 1984, *Proceedings of Moment Formation in Solids, NATO ASI Series No. 117* (New York: Plenum).
[61] ALLEN, J. W., and MARTIN, R. M., 1980, *J. Phys., Paris*, **171**, C5.
[62] ANDERSON, P. W., 1981, *Valence Fluctuations in Solids*, edited by L. M. Falicov, W. Hanke and M. B. Maple (Amsterdam: North-Holland) p. 451.
[63] JULLIEN, J., FIELDS, J., and DONIACH, S., 1977, *Phys. Rev.* B, **16**, 4889.
[64] YAMADA, K., KEI YOSIDA, and HANZAWA, K., 1984, *Prog. theor. Phys., Osaka*, **71**, 450; DONIACH, S., 1987, *Phys. Rev.* **35**, 1814.
[65] RUDERMAN, M. A., and KITTEL, C., 1954, *Phys. Rev.*, **96**, 99.
[66] BENOIT, A., FLOUQUET, J., RIBAULT, M., FLOUQUET, F., CHOUTEAU, G., and TOURNIER, R., 1978, *J. Phys., Paris*, **39**, 2–94.
[67] BRANDOW, B. H., 1986, *Phys. Rev. B*, **33**, 215, and references within.
[68] RICE, T. M., and UEDA, K., 1985, *Phys. Rev. Lett.*, **55**, 995, 2093.
[69] FAZEKAS, P., 1988 (to be published).
[70] GUTZWILLER, M. C., 1965, *Phys. Rev.* A, **137**, 1726.
[71] YOSHIMORI, A., and KASAI, H., 1983, *J. Magn. magn. Mater.* **31–34**, 475.
[72] YAMADA, K., and KEI YOSIDA, 1986, *Prog. theor. Phys.*, **76**, 621; HANZAWA, K., KEI YOSIDA and YAMADA, K., 1987, *Prog. theor. Phys.*, **77**, 1116.
[73] SIEMANN, R., and COOPER, B. R., 1980, *Phys. Rev. Lett.*, **44**, 1015.
[74] SKRIVER, H. L., 1984, *The LMTO Method, Springer Series in Solid States Sciences, Vol. 41* (Berlin: Springer).
[75] ANDERSON, P. W., and BRINKMAN, W. F., 1978, *The Physics of Liquid and Solid He*, Part II, edited by K. H. Benneman and J. B. Kellerman (New York: Wiley); BRINKMAN, W. F., and RICE, T. M., 1970, *Phys. Rev.* B, **2**, 4302; VOLLHART, D., 1984, *Rev. mod. Phys.*, **56**, 99.
[76] VARMA, C. M., 1979, *Solid St. Commun.*, **30**, 537.
[77] HERBST, J. F., and WATSON, R. E., 1975, *Phys. Rev. Lett.*, **34**, 1395; HERBST, J. F., WATSON, R. E., and LINDGREN, I., 1976, *Phys. Rev.* B, **14**, 3265.
[78] HOUGHTON, A., READ, N., and WON, H., 1987, *Phys. Rev.* B, **35**, 5123.
[79] KADOWAKI, K., and WOODS, S. B., 1986, *Solid St. Commun.*, **58**, 507.